Pontifícia Universidade Católica do Rio de Janeiro

José Guilherme Porto Oliveira

A BIM-based Framework for Infrastructure Management: Integrating Structural Health Monitoring and ANN-Driven Damage Detection

Tese de doutorado

Thesis presented to the Programa de Pós-graduação em Engenharia Civil of PUC-Rio in partial fulfillment of the requirements for the degree of Doutor em Ciências – Engenharia Civil

Advisor: Elisa Dominguez Sotelino

Rio de Janeiro

April 2025

Pontifícia Universidade Católica do Rio de Janeiro

José Guilherme Porto Oliveira

A BIM-based Framework for Infrastructure Management: Integrating Structural Health Monitoring and ANN-Driven Damage Detection

Thesis presented to the Programa de Pós-graduação em Engenharia Civil of PUC-Rio in partial fulfillment of the requirements for the degree of Doutor em Ciências Engenharia Civil. Approved by the examination Committee.

Prof. Elisa Dominguez Sotelino
Advisor
Departamento de Engenharia Civil e Ambiental – PUC-Rio

Prof. Paulo Batista Gonçalves
Departamento de Engenharia Civil e Ambiental – PUC-Rio

Prof. Diogo Rodrigo Ferreira Ribeiro
IPP

Prof. Ricardo Carrazedo
USP

Prof. Giuseppe Miceli Junior
IME

Rio de Janeiro, April 11th, 2025

José Guilherme Porto Oliveira

Undergraduate in Civil Engineering at Federal Institute of Alagoas (IFAL) in 2018. M.Sc. Degree in Civil Engineering at Pontifical Catholic University of Rio de Janeiro (PUC-Rio) in 2020.

Bibliographic data

Oliveira, José Guilherme Porto

A BIM-based Framework for Infrastructure Management: Integrating Structural Health Monitoring and ANN-driven Damage Detection / José Guilherme Porto Oliveira; advisor: Elisa Dominguez Sotelino. – 2025.
96 f.: il. color.; 30 cm

Tese (doutorado)–Pontifícia Universidade Católica do Rio de Janeiro, Departamento de Engenharia Civil e Ambiental, 2025.
Inclui bibliografia

1. Engenharia Civil e Ambiental - Teses. 2. SHM. 3. Detecção de danos. 4. Redes neurais artificiais. 5. BIM. 6. Manutenção de Infraestruturas. I. Sotelino, Elisa Dominguez. II. Pontifícia Universidade Católica do Rio de Janeiro. Departamento de

CDD: 624

To my family, for their support
and encouragement during this long journey.

Acknowledgments

To my parents, Genivaldo and Marisete, who tirelessly supported my education and instilled in me the values that guide my life. I owe everything to you.

To my wife, Ana Luiza, for your unwavering support and strength throughout this journey. Your courage has been my constant inspiration. To my brother, Gustavo, thank you for your visits, which brought me comfort and reminded me of home.

To Prof. Elisa Sotelino, my advisor, for her generosity, patience, and trust in my work. I am deeply grateful for your guidance, which helped me in shaping this thesis.

To the professors in the graduate program, for sharing your knowledge and enriching my academic journey.

To my friends, who stood by me during this phase and shared both the most challenging and joyful moments.

This study was financed in part by the Coordenação de Aperfeiçoamento de Pessoal de Nível Superior – Brasil (CAPES) – Finance Code 001

Abstract

Oliveira, José Guilherme Porto; Sotelino, Elisa Dominguez (Advisor). **A BIM-based Framework for Infrastructure Management: Integrating Structural Health Monitoring and ANN-Driven Damage Detection.** Rio de Janeiro, 2024. 96 p. Doctoral thesis – Department do Civil and Environmental Engineering, Pontifical Catholic University of Rio de Janeiro.

Bridges and viaducts play a critical role in urban infrastructure, ensuring mobility and supporting essential logistical chains. Their exposure to weather, dynamic loads, and aging requires continuous monitoring, as undetected damage can eventually develop into costly structural failures. Traditionally, visual inspections are used for evaluation, but they face limitations: difficulty accessing critical areas and subjectivity in defect interpretation, which depends on the inspector's expertise. Structural Health Monitoring (SHM) systems have emerged as alternatives, using dynamic properties (natural frequencies and mode shapes) to identify changes in structural stiffness. However, environmental factors such as thermal variations interfere with these properties, necessitating methods to distinguish external effects from actual damage. In this context, integrating Building Information Modeling (BIM) and digital twins represents a strategic advance in asset management, enabling the centralization of multidisciplinary data (design, intervention history, inspections) and their association with updatable numerical models to create a dynamic, intelligent infrastructure representation. This work proposes an innovative framework combining SHM, machine learning, and a BIM-based framework to optimize bridge management, focusing on early damage detection and reducing human uncertainty. The methodology was validated through a case study on the Rio Claro overpass (SP-340), which underwent environmental two vibration tests performed 10 years apart. A finite element model (FEM), was developed and updated using the experimental data with the objective of replicating the structure´s dynamic behavior. The calibrated model was used to simulate artificial damage at various positions and intensities. Modal curvatures, damage-sensitive features derived from vibration mode shapes, were extracted from simulated cases to train artificial neural networks (ANNs) for damage localization and severity estimation. The ANNs achieved classification accuracy exceeding 90%, thus, validating their effectiveness in filtering environmental interference. The

pre-digital twin, developed from a BIM model enriched with historical, technical, and inspection data, was integrated with the ANNs via a Python script, automating integrity reports based on field data and enabling interactive 3D visualization of structural conditions. The results demonstrate that the proposed approach not only improves diagnostic accuracy but also consolidates fragmented information into a single platform, facilitating predictive maintenance decisions, which can help extend the asset's service life. It is intended to provide an intuitive user interface so that asset managers can make data-driven decisions, overcoming the limitations of traditional visual inspections. This research attempts to bridge the gap between BIM and SHM applications by offering a replicable, efficient solution for infrastructure management.

Keywords

SHM; Damage Detection; Artificial Neural Networks; BIM; Building Information Modeling; Infrastructure Maintenance.

Resumo

Oliveira, José Guilherme Porto; Sotelino, Elisa Dominguez (Orientadora). **Uma Plataforma Baseada em BIM para Gestão de Infraestrutura: Integrando Monitoramento de Integridade Estrutural e Detecção de Danos Orientada por RNA**. Rio de Janeiro, 2025. 96 p. Tese de Doutorado – Departamento de Engenharia Civil e Ambiental, Pontifícia Universidade Católica do Rio de Janeiro.

Pontes e viadutos desempenham papel crítico na infraestrutura urbana, garantindo mobilidade e sustentando cadeias logísticas essenciais. Sua exposição a intempéries, cargas dinâmicas e envelhecimento demanda um cuidado contínuo, uma vez que danos não detectados precocemente podem evoluir para falhas estruturais custosas. Tradicionalmente, inspeções visuais são utilizadas para avaliação, mas enfrentam limitações: dificuldade de acesso a áreas críticas (como vãos elevados) e subjetividade na interpretação de defeitos, dependente da experiência do profissional. Sistemas de Monitoramento da Saúde Estrutural (SHM) surgem como alternativa, utilizando propriedades dinâmicas (frequências naturais e formas modais) para identificar alterações na rigidez da estrutura. No entanto, fatores ambientais, como variações térmicas, interferem nessas propriedades, exigindo métodos capazes de distinguir entre efeitos externos e danos reais. Nesse cenário, a integração de Modelagem da Informação da Construção (BIM) e gêmeos digitais apresenta-se como avanço estratégico para a gestão de ativos, pois permite centralizar dados multidisciplinares (projeto, histórico de intervenções, inspeções) e associá-los a modelos numéricos atualizáveis, criando uma representação dinâmica e inteligente da infraestrutura. Este trabalho propõe uma estrutura de trabalho inovadora que combina SHM, aprendizado de máquina e uma plataforma baseada em BIM para otimizar a gestão de pontes, focando na detecção precoce de danos e na redução de incertezas humanas. A metodologia foi aplicada a um viaduto em Rio Claro (SP-340), submetido a ensaios de vibração ambiental em dois instantes, com intervalo de 10 anos entre eles. Um modelo de elementos finitos (MEF) foi desenvolvido e calibrado usando dados experimentais, com o objetivo de replicar o comportamento dinâmico da estrutura. O modelo ajustado foi utilizado para simular danos artificiais em diversas posições e intensidades. Curvaturas modais, extraídas das formas de vibração dos casos

simulados, compuseram um banco de dados para treinar redes neurais artificiais (RNA), responsáveis por localizar danos e estimar sua severidade. As RNAs alcançaram acurácia superior a 90%, validando sua eficácia na filtragem de interferências. O gêmeo digital prévio, desenvolvido a partir de um modelo BIM enriquecido com dados históricos, técnicos e de inspeção, foi integrado às RNAs por meio de um Script Python, automatizando a geração de relatórios de integridade baseados em dados de campo e permitindo visualização 3D interativa das condições estruturais. Os resultados demonstram que a abordagem proposta não apenas melhora a precisão do diagnóstico, mas também consolida informações fragmentadas em uma plataforma única, facilitando decisões de manutenção preditiva e que podem ajudar a prolongar a vida útil do ativo. Pretende-se com a estrutura de trabalho proposta prover uma interface intuitiva para que gestores de ativos de infraestrutura possam tomar decisões baseadas em dados, superando parte das limitações decorrentes das inspeções tradicionais. Este trabalho tenta suprir uma lacuna entre o método BIM e ferramentas SHM oferecendo uma solução eficaz e replicável para a gestão de infraestruturas.

Palavras-chave

SHM; Detecção de Danos; Redes Neurais Artificiais; BIM; Manutenção de Infraestruturas.

Table of contents

List of figures

1
Introduction

1.1.
Motivation

Bridges and viaducts are essential for regional infrastructure, facilitating logistics and urban transportation. Although they are structures are designed to last, their lifespan depends on regular maintenance based on periodic inspections, as their load-bearing capacity decreases over time. Vehicle traffic and environmental factors can cause small cracks, which, if not detected early, may grow larger [1]. Managers strive to carry out efficient and cost-effective maintenance, but this is only achievable through early problem detection, which depends on thorough and high-quality inspections.

Condition inspections of these structures are usually conducted through visual assessment. According to An *et al.* [2], this approach presents two main drawbacks: the difficulty in accessing certain locations and the subjectivity of the evaluation. The inspector may be unable to reach certain areas of the structure due to its height or structural arrangement, which can hinder the identification of critical defects. Additionally, the assessment relies on the inspector's personal experience, introducing a subjective factor that could affect the reliability of the results. As an additional safety layer to these challenges, Structural Health Monitoring (SHM) systems have been developed, allowing for early damage detection and reducing the subjectivity factor in the structural evaluation [3].

SHM technologies employ non-destructive techniques to detect structural defects by analyzing changes in its dynamic properties, such as natural frequencies and vibration modes [4]. Two main approaches to damage detection have been used: data-driven and model-based. Data-driven systems rely on continuously monitored sensor data to identify deviations in a structure's physical or mechanical behavior [5]. By applying statistical analysis and advanced mathematical methods, this approach compares baseline (undamaged) and updated (potentially damaged) structural states to assess integrity. In contrast, the model-based methodology uses theoretical or empirical data to create mathematical or physical models, often calibrated finite element models (FEMs), that simulate structural behavior under various damage scenarios and operational conditions. Environmental factors, such as temperature fluctuations and wind,

complicate damage detection by inducing changes in modal properties that may resemble structural degradation. Machine learning (ML) algorithms have become instrumental in addressing this challenge. When trained on comprehensive datasets, these algorithms excel at distinguishing environmentally induced variations from genuine damage, enhancing the reliability of SHM systems. By integrating machine learning, SHM frameworks gain improved pattern recognition capabilities, enabling earlier and more accurate identification of structural anomalies [6].

To make effective decisions regarding infrastructure maintenance, managers need more than information about the current condition of assets. Documents such as original designs, construction reports, and inspection and maintenance records are essential to complement the data provided by SHM systems. When these documents are only available in paper form, there is a high risk of losing important information, which greatly hinders effective infrastructure management. An efficient solution to this issue is to create a centralized digital database where all this information can be stored, organized, and easily accessed. Building Information Modeling (BIM) is a methodology that involves creating and managing detailed, information-rich digital representations of built assets, including buildings and bridges. This collaborative approach integrates data and processes in a standardized digital environment, facilitating decision-making throughout the project's lifecycle [7]. Bridge Information Modeling (BrIM), an extension of BIM, is specifically applied to modeling and management of bridges, enabling an integrated and specialized digital approach for these structures. With the evolution of BIM, the concept of a digital twin emerged - an updated virtual representation of a physical object that simulates its behavior and performance.

This study proposes and implements a methodology that combines an SHM system, powered by artificial neural networks, within a Building Information Modeling framework. The approach is hybrid, leveraging both field tests and numerical models to create a robust and reliable damage prediction tool. By integrating SHM and BIM, this research addresses a critical gap in the literature while also tackling practical challenges, such as workflow and interoperability across platforms.

1.2. Objectives

This work aims to develop and evaluate a BIM-based method for creating a pre-digital twin which integrates a structural health monitoring (SHM) system powered by artificial neural networks. The framework relies on an experimentally validated numerical model that is integrated with a BIM platform.

To achieve the expected result, the work established the following goals. Regarding the experimental part of the work, it is expected:

- Characterize the viaduct's modal properties through ambient vibration tests, employing different methods to analyze the acquired data and evaluate this redundancy layer's effectiveness.
- Compare the modal properties obtained from tests conducted at different times under similar conditions to identify whether there have been significant changes and assess their implications.

The numerical approach of the work involves developing a calibrated finite element model and two artificial neural networks for structure condition assessment. Regarding the numerical modeling component, the goals are:

- To evaluate different modeling strategies in terms of their similarity to the field results. Once established the accuracy of each modeling technique, assess their performance with regards to database generation.
- Perform a sensitivity analysis in the manual adjustment of the finite element model, identifying which calibration parameters most significantly influence the results.
- Develop two neural networks capable of diagnosing, locating, and estimating the extent of damage and of evaluating their performance. These prediction models are the diagnosis system's core and are fed by field test results.

The third part of the work addresses the integration of the developed tools into a workflow that uses the BIM methodology, ultimately creating the case study viaduct pre-digital twin. In this stage, the goals are:

- Propose and describe the workflow, identifying the actors involved in integrating a Structural Health Monitoring (SHM) tool into an enriched information model through the BIM methodology. Apply the method to a case study and evaluate its feasibility based on practical criteria.
- Enrich the model with relevant information for structure management and ultimately assess its integration into the workflow.

1.3. Organization

The thesis is structured in manuscript format, and some chapters consist of excerpts from articles accepted for publication or submitted for publication in international peer-reviewed journals for which the author of this thesis is the first author.

Chapter two presents the theoretical framework that supports the thesis. In this section, the mathematical formulation of operational modal analysis methods is detailed, as well as the concepts of the two damage indicators used in the study. Additionally, aspects related to the adjustment of finite element models and the construction and evaluation of artificial neural networks for structural health analysis are addressed. The third chapter describes the systematic literature review, detailing methods and criteria used to select the articles that formed the basis of the research. Finally, the main results found are presented and discussed, as well as the gaps identified in the literature. Chapter four provides a detailed description of the methodology used in the thesis. This section outlines the various stages of the research, explains how each stage was carried out, and specifies the evaluation criteria applied to assess the outcomes of each phase.

The last five chapters of this thesis are structured using excerpts from the papers “An Infrastructure Management Framework Using a Digital Twin, Integrating SHM and BIM”, “Damage Detection in Reinforced Concrete Bridge: An ANN-Based Approach for Inspection”, and “Dynamic Testing and Finite Element Model Updating for a Viaduct Structural Assessment” [8].

Chapter five introduces the proposed framework for infrastructure management using digital twins, detailing each step of its implementation. Chapter six describes the experimental program, covering the case study and the results of two experimental campaigns conducted in collaboration with researchers of USP, São Carlos and PUC-Rio to obtain the structure’s modal properties. Chapter seven focuses on finite element modeling strategies and the model updating process. Chapter eight explores the damage diagnosis tool based on artificial neural networks in detail. Chapter nine presents the integration of the SHM (Structural Health Monitoring) tool with the BIM (Building Information Modeling) environment. Each chapter concludes with findings related to its respective topic. Finally, chapter ten concludes the thesis by providing the main conclusions from the work and presenting some recommendations for future research.

2.
Theorical background

2.1.
Operational modal analysis

The modal data acquisition of a system is generally performed by two methods: classical Experimental Modal Analysis (EMA), where both inputs and outputs are measured with appropriate transducers, and Operational Modal Analysis (OMA), where only the structure's response to actions resulting from its usage is measured. In civil engineering structures, which typically have large dimensions, applying forced vibrations can pose challenges, such as disrupting usage or encountering very low-frequency vibration modes that are difficult to identify with existing excitation equipment. Performing Ambient Vibration Tests (AVT) presents an alternative that eliminates the need for force application equipment. As a result, these tests are cheaper, faster, and do not interfere with the structure's regular use [9, 10].

From the test-collected signals, it is possible to extract modal parameters, such as natural frequencies, mode shapes, and damping ratios, using different techniques. This phase in modal analysis is known as Modal Identification. There are several modal identification techniques available that utilize data from ambient vibration tests [11]. Naturally, employing multiple identification methods ensures greater confidence in the results [12]. Among the well-known frequency-domain methods are the Frequency Domain Decomposition (FDD) method and its enhanced version, the Enhanced Frequency Domain Decomposition (EFDD) [13]. In addition, time-domain identification algorithms, essentially based on either stochastic state-space models or Auto-Regressive Moving Average (ARMA) models, are also widely used in OMA. Stochastic Subspace Identification (SSI) techniques, such as the Covariance-driven SSI (SSI-COV) method, are prevalent in civil engineering applications. This paper will explore and discuss these methods in detail.

2.1.1.
Enhanced Frequency Domain

Frequency Domain Decomposition is an output-only system identification technique introduced by Brincker *et al.* [14] and subsequently enhanced to extract

modal damping factor estimates. As an extension of the FDD method, EFDD also employs Singular Value Decomposition (SVD) algorithms to diagonalize the matrix of spectral density functions and detect mode multiplicity. This process decomposes the spectral matrix into auto-spectral density functions, each corresponding to a single degree of freedom (SDOF) system. Understanding the theoretical background of this method requires starting with the relationship between the unknown inputs, $x(t)$, and the measured responses, $y(t)$, which, according to Bendat *et al.* [15], are expressed as eq. 1:

$$\left[G_{yy}(j\omega)\right] = [H(j\omega)]^{*}[G_{xx}(j\omega)][H(j\omega)]^{T} \quad (1)$$

where $[G_{yy}(j\omega)]$ is the Power Spectral Density (PSD) matrix of the input, $[G_{xx}(j\omega)]$ is the PSD matrix of the responses, $[H(j\omega)]$ is the Frequency Response Function (FRF) matrix and the superscript * and superscript T denotes the complex conjugate and transpose, respectively. At a certain frequency $\omega = \omega_i$, applying SVD to the output PSD matrix results in eq. 2:

$$\left[\hat{G}_{yy}(j\omega_i)\right] = [U]_i[S]_i[U]_i^H \quad (2)$$

where $[U]_i$ is a unitary matrix holding singular vectors u_{ij}, $[S]_i$ is a diagonal matrix of singular values in descending order and the superscript H means a complex conjugate and transpose.

In this method, the natural frequencies are estimated by identifying a peak in the plot of singular values of the PSD matrix of the response, while the mode shapes are determined as the first singular vector u_{i1} at the corresponding frequency [16]. The modal damping ratios are extracted by analyzing the decay of the auto-correlation functions, which are evaluated by performing the inverse Fourier transform of the SDOF systems' PSDs and applying linear regression to the logarithmic decrement [17]. This process can be repeated for other peaks to estimate the modal damping ratios of additional modes [18].

2.1.2. Covariance-driven Stochastic Subspace Identification

There are several variants of Stochastic Subspace Identification (SSI) algorithms, which are widely used in operational modal analysis due to their high estimation accuracy, computational robustness, and efficiency [19]. One such

variant is the SSI-COV, a time-domain covariance-driven method classified as a parametric procedure. As its name implies, the SSI-COV algorithm requires that covariance functions are first estimated from raw output time histories [20]. This technique fits a model to the data, addressing the challenge of identifying a stochastic state-space model from output-only data, also referred to as stochastic realization problem. The stochastic state-space model is described by Qin *et al*. [21] as shown in eq. 3:

$$\begin{aligned} \{x_{k+1}\} &= [A]\{x_k\} + \{w_k\} \\ \{y_k\} &= [C]\{x_k\} + \{v_k\} \end{aligned} \tag{3}$$

where $\{x_k\}$ is the state vector; $\{y_k\}$ is the output vector (the measurements), $\{w_k\}$ and $\{v_k\}$ stand for the modeling errors and test inaccuracies, and $[A]$ and $[C]$ are the state matrix that characterizes the dynamics of the system through its eigenvalues and the output matrix that specifies how the internal states are transformed to the outside world [22], respectively. The main idea of this method is to identify these system matrices. To achieve this, the first step is determining the output covariance $[R_i]$, defined by eq. 4:

$$[R_i] = [C]\left[A^{i-1}\right][G] \tag{4}$$

here, $[G]$ represents the next state-output covariance matrix. Once the covariance sequence R_i is estimated from the measurement data, the next step is to decompose the covariances to determine the matrices $[A]$, $[C]$, and $[G]$. Thus, a block Toeplitz matrix $\left[T_{1|i}\right]$ $(li \times li)$, where l is the number of outputs is formed that consists of covariances matrices:

$$\left[T_{1|i}\right] = \begin{pmatrix} [R_i] & [R_{i-1}] & \cdots & [R_1] \\ [R_{i+1}] & [R_i] & \cdots & [R_2] \\ \cdots & \cdots & \cdots & \cdots \\ [R_{2i-1}] & [R_{2i-2}] & \cdots & [R_i] \end{pmatrix} = \begin{pmatrix} [C] \\ [CA] \\ \cdots \\ [CA^{i-1}] \end{pmatrix} \begin{pmatrix} [A^{i-1}] & [G] & \cdots & [AG] & [G] \end{pmatrix} = [O_i][\Gamma_i] \tag{5}$$

Eq. 4 demonstrates that the Toeplitz matrix can be decomposed into the product of the extended observability matrix $[O_i](li \times n)$, where n is the model order, and the reversed extended stochastic controllability matrix $[\Gamma_i](n \times li)$. The next step in the SSI-COV implementation involves computing the SVD of $\left[T_{1|i}\right]$ to obtain the expression shown in eq. 6, as showed by Peeters [23]:

$$\left[T_{1|i}\right] = [U][S][V]^T \quad (6)$$

where $[U]$ and $[V]$ are orthogonal matrices, while $[S]$ is a diagonal matrix containing the positive singular values in descending order. By simultaneously solving Equations (5) and (6), the system matrices, the system matrices $[A]$, $[C]$, and $[G]$ can be estimated. The modal parameters are then derived from the matrices $[A]$ and $[C]$, starting with the eigenvalue decomposition of the state matrix [A]. For applications in modal analysis, constructing a stabilization diagram by computing the SVD of the covariance Toeplitz matrix proves to be an effective method for eliminating spurious modes [23].

2.2.
Damage indicators

The choice of damage indicator in SHM systems is crucial for reliable damage detection, especially in the presence of environmental effects. The model-based and hybrid approaches share the use of damage indicators to identify changes in the structure's modal properties. An accurate damage indicator should be sensitive to structural changes caused by damage while being robust against changes due to environmental influences [24]. Natural frequencies are commonly used as damage indicators because they are easy to measure, although they are also significantly affected by environmental changes [1, 25]. Dynamic damage indicators are based on the principle that any alterations in a structure's physical properties - whether in its mass, damping, or stiffness - directly affect its modal characteristics, including natural frequencies and mode shapes. The development of a crack within a beam in an assembly leads to a decrease in stiffness. This change influences not only the vibrational characteristics of the beam itself but also the overall deformation pattern of the entire structure.

The modal curvature method (MCM) is an established damage index in structural analysis. This method, introduced by Pandey *et al.* [26], calculates the second derivative of modal displacement to assess structural damage. Its effectiveness has been documented across different bridge types. Studies have demonstrated its successful implementation in steel bridges, as shown by Nick & Aziminejad [27]. For reinforced concrete bridges, multiple researchers have validated its application, including the works of Abdel Wahab & De Roeck [28], Dilena *et al.* [29], Erduran *et al.* [30] and Sánchez-Aparicio *et al.* [31]. In one-dimensional applications, after the structure is discretized into elements of length

h, the modal curvature can be computed using a centered difference scheme, as shown in eq. (7).

$$k_i = (w_{i+1} + w_{i-1} - 2w_i)/h^2 \tag{7}$$

where w_i to represent the modal displacement at position i. To determine structural damage, the method compares the modal curvatures of the structure in both its damaged and undamaged states. This comparison is expressed mathematically in eq. (8), where the damage index is calculated as the difference between these curvatures.

$$\Delta k = \sum_{i=1}^{n} k_i - k_i^* \tag{8}$$

where k_i denotes the undamaged curvature, k_i^* denotes the damaged curvature, and n represents the number of mode shapes considered. The physical meaning of the MCM, as explained by Pandey et al. [26], lies in its ability to indicate localized changes in a structure due to damage. When a structural element experiences damage, such as a crack, it leads to a reduction in its flexural stiffness (EI), which in turn increases the curvature at that damaged section. Therefore, the difference in modal curvature between an intact and a damaged structure serves as a precise measure of how damage alters stiffness and structural behavior at specific locations. This change is localized, effectively highlighting the area of damage.

Another important damage index for bridges and viaducts is obtained from the modal strain energy (MSE) change, which was initially proposed by Stubbs & Kim [32]. For framed and plate-like structures, this strain energy can be obtained using the MCM, as shown in eq. (9), and it can be used as a damage indicator by its normalized index given by eq. (10),

$$\beta_j = \frac{\sum_{i=1}^{m}\left[\left(\int_j (k_i^*)^2 dx + \int_0^L (k_i^*)^2 dx\right)\int_0^L (k_i)^2 dx\right]}{\sum_{i=1}^{m}\left[\left(\int_j (k_i)^2 dx + \int_0^L (k_i)^2 dx\right)\int_0^L \left(k_i^*\right)^2 dx\right]} \tag{9}$$

$$Z_j = \frac{\beta_j - \overline{\beta_j}}{\sigma_\beta} \tag{10}$$

where k_i and k_i^* are the undamaged and damaged ith mode shape curvature at the element j, m is the bending mode shape, β_j is the modal strain energy in the element j, ($\overline{\beta_j}$) is the mean of β_j results and σ_β is its standard deviation. The modal strain energy index was successfully applied as damage indicator for reinforced concrete bridges [33, 34], steel-concrete composite structures [35] and truss-like bridge [36]. An alternative, in addition to the two previous methods, is the modal flexibility index. The technique combines natural frequencies and mode shape displacements to find damage in structures and has also been explored as a damage indicator in other works [37, 38].

Damage indicators are effective in detecting and locating damage. Depending on the application one index may outperform another. Also, many authors report the results for simpler structures such as beams or frames [39–41]. Authors, such as dos Santos Mota *et al.* [42] evaluated the application of these indices to detect and locate damage in full-scale 3D pedestrian bridges. They concluded that for these complex structures, the strain energy index produced the best results.

2.3.
Finite elements model adjustment

Manual model calibration offers greater flexibility to the analyst, allowing for precise and iterative adjustments to the model and has demonstrated effectiveness in previous studies [43–45]. The selection of parameters to be adjusted is crucial and depends on the analyst's expertise, allowing them to make a judicious selection based on real physical data and avoid arbitrary adjustments [46]. Both static and dynamic tests can provide data for model calibration. The need for traffic interruption makes static tests, though important for calibrating boundary conditions and element stiffness, logistically challenging. On the other hand, dynamic tests, which capture the global behavior of the structure under operational conditions [24], are more commonly used in practice [47–50]. Few studies, such as [44, 51, 52], have explored the combination of both types of tests, despite the potential to enhance model update quality.

To evaluate the output progress at each step, it is common to compare natural frequencies measured in the field against those obtained through numerical calculations. According to Talebi *et al.* [45] this comparison can be quantified using the objective function described in eq. 11:

$$\varepsilon = \frac{\left|f_i^{exp} - f_i^{num}\right|}{f_i^{num}} \tag{11}$$

where i represents the analyzed vibration mode, while f_i^{exp} and f_i^{num} denote the experimental and numerical frequency values, respectively.

In dynamic analysis, the Modal Assurance Criterion (MAC) serves as a key indicator for measuring correlation between different vibration mode shapes. As noted by Allemang [53], higher MAC values indicate stronger correspondence between the compared modes. The MAC index is mathematically expressed as shown in eq. 12:

$$MAC(\phi_i, \phi_j) = \frac{\left|\phi_i^T \phi_j\right|^2}{(\phi_i^T \phi_i)(\phi_j^T \phi_j)} \tag{12}$$

where ϕ_i and ϕ_j denote the modal displacements associated with vibration modes i and j, respectively, and ϕ_i^T and ϕ_j^T represent their corresponding transposed forms. When analyzing the MAC matrix, the main diagonal elements show how each mode correlates with itself, while off-diagonal elements indicate a correlation between different modes. For optimal mode separation, the off-diagonal elements should exhibit low values.

The Modal Match Index (MMI) is a metric used to simultaneously evaluate the similarities between modal shapes and natural frequencies [4]. The MMI provides a single value that indicates how closely two vibration modes align in terms of natural frequency and mode shape, as described by eq 13:

$$MAC(\phi_i, \phi_j) = \frac{\left|\phi_i^T \phi_j\right|^2}{(\phi_i^T \phi_i)(\phi_j^T \phi_j)} \tag{13}$$

where γ is a value between 0 and 1 that assigns weight to the relevance of modal shapes and natural frequencies in the calculation. $MAC_{i,j}$ represents the MAC values between the experimental (i) and numerical (j) modes. f_i and f_j are the experimental and numerical natural frequencies for the analyzed mode. The MMI is particularly useful during the model validation and updating process, helping to assess whether adjustments made to a numerical model reach better agreement with experimental data.

2.4.
Artificial neural networks

Artificial Neural Networks, particularly multilayer perceptron (MLP), operate by passing input data through multiple interconnected neurons layers, applying a weighted sum and a non-linear activation function to produce an output (Figure 1). The operating sequence starts with the input layer, followed by one or more hidden layers, and finally the output layer. Activation functions like ReLU (Rectified Linear Unit), sigmoid, and tanh are responsible for activating or not an artificial neuron and for introducing non-linearity into the model, enabling it to capture complex patterns. During the network training phase, key parameters include the learning rate, which controls the step size in the weight update process, and the number of epochs, which determines how many times the entire training dataset is used. Training means adjusting the network's weights and biases to minimize the error between predicted and real output values, a process guided by the backpropagation algorithm. Gradient descent is a commonly applied optimization technique also applied in this step, which iteratively updates the network's parameters in the direction of the negative gradient of the loss function to find the minimum error. ANNs excel at handling large amounts of data due to their ability to learn complex patterns.

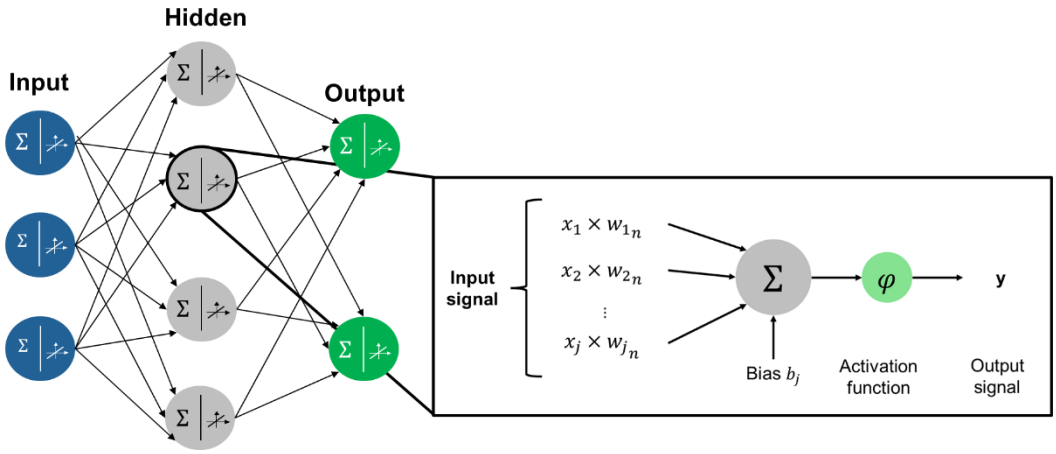

Figure 1 - MLP structure

3.
Systematic literature review

3.1.
Methodology

The systematic literature review sought works that integrated SHM tools with the BIM method for infrastructure management. According to Webster and Watson [54], a systematic literature review facilitates the development of theories, avoiding focus on heavily explored areas and pointing to gaps in knowledge. This becomes possible due to the clarity and replicability of the procedure through criteria and methods.

To reach the desired articles, the systematic literature review followed the method proposed by Pati *et al.* [55], which divides the search into three phases: formulation of the question to be answered, the location of the articles, and the analysis of the results. Following the method, a question to be answered by the review was initially defined: "How are SHM tools integrated with the BIM method for infrastructure management and damage assessment?". Through the selection of articles in the area, an attempt was made to understand the state of the art in this field and thus define the path followed by the research. The word tree constructed from the research question is illustrated in Figure 2 and represents an ideal search scenario.

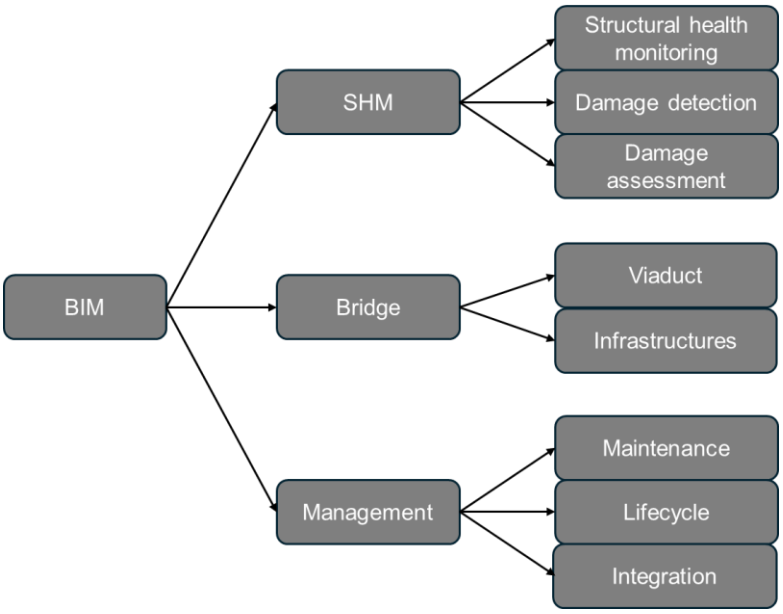

Figure 2 - Word tree

The word tree was used to create a set of initial keywords for the hunt. Searches were conducted in the Scopus and Web of Science databases, testing different strings to optimize the number of relevant results (Table 1). To ensure a focused analysis, duplicate publications were excluded and the search was limited to journal articles published between 2017 and 2024, a representative time window for the theme. Initially, only the keywords from the word tree were used, which resulted in 15 works. To expand the results, the search was refined with the inclusion of synonyms and complete expressions, raising the total to 25 works.

Table 1 - Search strings

Initial string	**Final string**
(“BIM” OR “Building information modeling”) AND (“SHM” OR “Structural health monitoring”) AND (“Bridge” OR “Viaduct”) AND (“Management” OR “Maintenance”)	(“BIM” OR “Building information modeling” OR “BrIM” OR “Bridge information model”) AND (“SHM” OR “Structural health monitoring” OR “Damage assessment” OR “Damage detection”) AND (“Bridge” OR “Viaduct”) AND (“Management” OR “Maintenance” OR “Lifecycle management”)

To better filter the papers that actually studied the integration between the SHM with BIM methodology for infrastructure management and damage assessment, the following three-stage filtering process was performed: (1) Reading titles and abstracts, (2) Reading conclusions, (3) Reading the full article.

3.2. Findings

After implementing the filtering protocol described earlier, 25 works were selected for review. Among them, 3 were literature reviews, and 3 did not directly focus on damage assessment. The remaining 19 works were fully analyzed. Additionally, 3 more articles were incorporated into the database using the snowballing technique. Table 2 summarizes these works, highlighting relevant information, such as: the adopted BIM environment, the damage assessment strategy and the integration between them.

Table 2 - SLR findings

Reference	BIM environment	Damage assessment strategy	Integration
McGuire *et al.* [56]	Revit	Visually detected by inspectors.	A tool within the BIM environment allows inspectors to document the location of damage. The tool uses parametric geometries (damage cubes) to represent the volume and severity of damage.
McKenna *et al.* [57]	Revit	Visually detected by 3D terrestrial laser scanning.	Embedding condition rating parameters within the BrIM model.
Sacks *et al.* [58]	Revit / Leap Bridge	Image analysis.	The generation of an 'Inspection BIM Model', which includes defect data located on bridge component surfaces.
Wan *et al.* [59]	Revit	Visually detected by inspectors.	Incorporating a monitoring module that tracks and evaluates the condition of bridge components according to regular statistics and reports
Boddupalli *et al.* [60]	Revit	SHM data-driven system	Linking sensor data collected from the structure to the BIM model.
Singh and Sadhu [61]	Revit	SHM data-driven system	Linking sensor data collected from the structure to the BIM model.
Kwon *et al.* [62]	Revit	SHM ANN-driven system	Using the IFC spatial elements to connect the measured sensor data and the predicted normal values with the digital representation of the bridge.

Reference	BIM environment	Damage assessment strategy	Integration
Kaewunruen *et al.* [63]	Revit	Visually detected by inspectors.	Embedding the assessment results directly into the 3D model.
Hamdan *et al.* [64]	OpenBridge	Image analysis.	Linking the derived geometric data from the point clouds and the semantic representations of the recorded damages within the BIM model.
Yamane *et al.* [65]	Revit	Image analysis.	The 3D positions of the detected damages were reflected in the BIM model as attributes, which included links to images and damage type details.
Li *et al.* [66]	Revit	SHM data-driven system	The damage detection strategy was integrated into the BIM environment through a monitoring data parsing function.
Truong *et al.* [67]	Revit	SHM model-based system	Linking the results analyzed in Microsoft Excel with the Dynamo tool in Revit
Talebi *et al.* [45]	Revit	Modal properties changes	Utilizing vibration data collected from dynamic tests to update the geometric and structural information present in the BIM model
Petti *et al.* [68]	Revit	Visually detected by inspectors.	Through a Bridge Management System (BMS), external to Revit, designed to enable real-time monitoring and data collection related to bridge conditions.

Reference	BIM environment	Damage assessment strategy	Integration
Mohammadi *et al.* [69]	Revit	Visually detected by 3D terrestrial laser scanning.	Utilizing algorithms that calculate a condition index according to the damage severity.
Mohamed *et al.* [70]	Revit	Visually detected by inspectors.	Incorporating inspection data into the BrIM design, allowing for structural defects visualization in the model.
Fawad *et al.* [71]	Revit	SHM model-based system	Deploying sensors, such as strain gauges and accelerometers, into the BIM model.
Gragnaniello *et al.* [72]	OpenBridge	SHM data-driven system	Through a code that utilizes Levels of Information Need (LoINs) and the BIM model as input to incorporate sensor data to the model.
Hagedorn *et al.* [73]	OpenBridge	Visually detected by inspectors.	Through the use of Information Containers (ICDD).
Aziz *et al.* [74]	Revit	SHM data-driven system	Using a data-driven approach where asset data is captured, developed, and enriched consistently within the BIM framework.
Alsharif *et al.* [75]	Revit	SHM model-based system	Through the use of Python scripts in Dynamo, which generate the DIM (Damage Information Model).

From Table 2, it is possible to draw some conclusions about the state of the art in integrating SHM systems and infrastructure management with the BIM methodology. It is observed that Revit is the most widely used BIM environment for this integration, mainly due to its compatibility with accessible programming languages, such as Python, through the native Dynamo library. This compatibility facilitates integration with external systems and enables the creation of more user-friendly interfaces, contributing to its widespread adoption.

Another relevant point is that most of the analyzed studies rely exclusively on conventional visual inspections for damage detection and recording. Although a variety of SHM systems have been implemented in the remaining studies, only one employs artificial neural networks for infrastructure damage detection. This finding highlights a gap yet to be explored, considering the potential of ANNs to process large volumes of data and identify complex patterns.

Furthermore, most of the reviewed studies are limited to importing sensor data into the BIM environment or using it solely as a space for recording detected damage. However, decision-making regarding interventions in an infrastructure should consider not only its current condition but also its maintenance history. In this regard, there is a significant absence of methodologies that integrate a comprehensive historical record, going beyond damage registration and incorporating data relevant to the asset's service life.

Digital Twins (DTs) are defined as virtual models that replicate the characteristics and behavior of physical assets, using data and models to simulate their performance and service life [76]. According to Kritzinger [77], three types of digital twins are highlighted by: Digital Mirror, which is a static representation of the asset without connection to real-time data; Digital Shadow, which allows a unidirectional data flow from the physical asset to the virtual model; and Digital Twin, which enables bidirectional data exchange, allowing scenario simulation and decision-making based on updated data. In viaduct management, BIM is used to plan, execute projects, and store information and maintenance records. At the same time, digital twins allow monitoring of the structure's condition, optimizing maintenance interventions and operation. Honghong *et al.* [78] define Digital Twin types based on data-collection frequency and system-automation level. A pre-Digital Twin (pre-DT) is a static model of a physical asset—such as a building or bridge—updated only at set intervals to record its design, specifications, and past operational data. By contrast, an ideal Digital Twin continuously ingests real-time sensor data and other information, delivering dynamic, actionable insights. The key distinction is that a pre-DT cannot portray live operating conditions, whereas an

ideal DT supports proactive decision-making through uninterrupted monitoring and automated analytics.

The application of BIM in infrastructure has shown promising results in infrastructure engineering. In asset management, works such as [7, 73, 79] concluded that BIM optimizes processes, centralizes information, and enables a holistic view of the infrastructure lifecycle, facilitating strategic decision-making. In data management, [7, 56, 74, 75] demonstrated that the methodology provides a unified platform for efficiently storing and analyzing information, supporting maintenance interventions. Infrastructure health monitoring is significantly enhanced by integrating up-to-date data, allowing for quick response to adverse events [62, 67, 71, 72]. Finally, the adoption of the methodology allowed for new inspections methods by providing visual and analytical tools that increase the accuracy and efficiency of this process [61, 70, 80].

Digital twins have been successfully used for several activities. This tool, when powered by IoT (Internet of Things) sensors, enables continuous monitoring of various structural parameters [81–84]. By collecting and presenting real-time data, these virtual models allow early damage detection and accurate assessment of building integrity. Other works, such as those by [85, 86], tested the behavior of the structure in different scenarios, including extreme load applications, environmental changes, and wear effects over time through digital twins. This visualization capability allows the identification of critical points, evaluation of different cases effectiveness, and optimization of structural performance.

4.
Methodology Overview

4.1.
Modal properties assessment

Two distinct techniques of Operational Modal Analysis (OMA) were employed to obtain the modal properties of the case study viaduct: EFDD and SSI-COV. The EFDD technique is based on the decomposition of power density spectra through Singular Value Decomposition (SVD), allowing for precise identification of peaks corresponding to natural frequencies and the extraction of associated mode shapes. In parallel, the SSI-COV method, operating in the time domain, uses covariance matrices to build estimated state models, enabling robust identification of the structure's dynamic parameters. The combined use of these approaches seeks to reinforce the reliability of the results and allows for cross-validation of the extracted modal parameters, ensuring precision in characterizing the dynamic behavior of the structure.

The correct mode shapes identification is essential for calculating the damage indicators chosen for the work and depends on the robustness of the experimental mesh adopted in the ambient vibration tests. To faithfully capture the spatial variations of the structural response, it is essential to use a dense and well-distributed experimental mesh that ensures the capture of necessary details for defining the mode shapes. This experimental configuration minimizes the effects of noise and environmental interference, in addition to avoiding errors resulting from undersampling, contributing to the previously mentioned modal identification methods operating under ideal conditions. The robustness of the experimental mesh is a fundamental element to be evaluated in this work to ensure obtaining reliable data.

4.2.
Finite elements modeling criteria

Three different modeling techniques were investigated to determine the one that best captured the behavior of the physical structure. All models were developed using the Abaqus software [92]. The evaluated model arrangements were selected based on the results obtained by Chung & Sotelino [87], in which the modeling of similar viaducts was studied. However, since they considered only

the structural response due to static loads, further investigation was necessary to verify which arrangement best captures the structure's dynamic behavior. In Model A, the longitudinal girders, transverses, and abutments were modeled using three-dimensional beam elements (Figure 3a). These beam elements feature a full six degrees of freedom per node (three translational and three rotational), enabling them to accurately capture bending, shear, axial, and torsional responses.. The deck was modeled using quadratic thick shell elements (S8R). This eight-node shell formulation is specifically designed to incorporate thickness effects and provides enhanced kinematic capabilities to effectively model both membrane and bending behaviors. In Model B, all structural elements were modelled using S8R elements. Both Models A and B used rigid links to join the centroids of the longitudinal beams and the deck (Figure 3b). Model C used quadratic solid elements (C3D20) to model all structural elements. These elements provide a high level of discretization for the simulation of the three-dimensional stress distribution across the structure, with each node possessing three translational degrees of freedom.

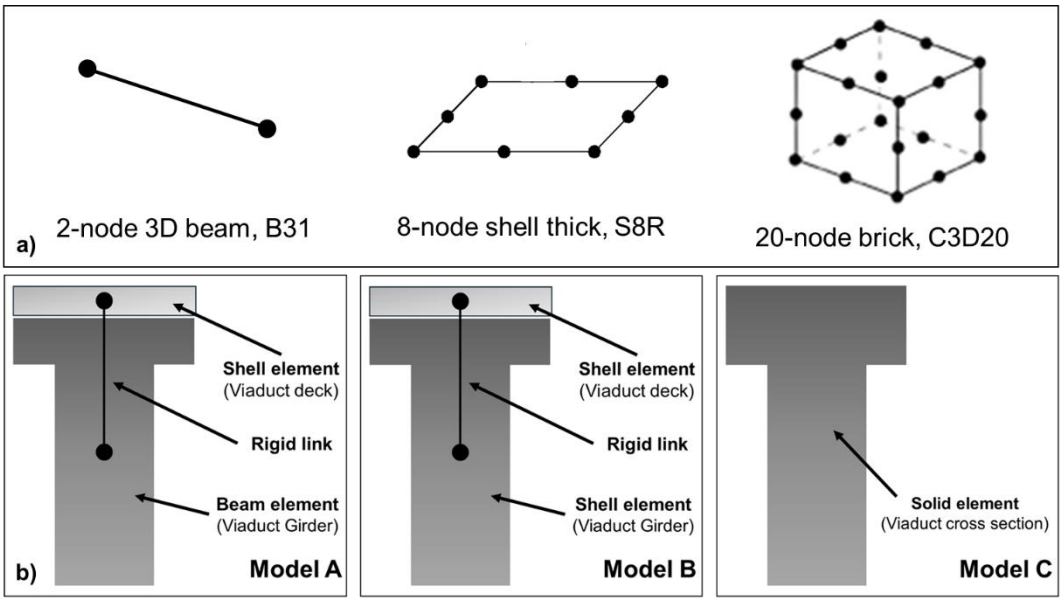

Figure 3 – a) Employed elements b) FE model arrangements

In general, model adjustment can be accomplished automatically or manually. Both strategies have the same objective: to make the model's behavior mimic the observed in the field tests. The difference between them relies on the way this result is reached. While the first strategy adopts an optimization algorithm to promote the properties changes in the elements, the second depends on the modeler's experience to appropriately change properties to modify the global

structural response. Since the focus of this study are viaducts composed of simple structural arrangement and built with a single material, manual model updating was selected. The natural frequency values and vectors of the modal displacements, experimentally obtained, are used as reference values for the variables f_i^{exp} and ϕ_j in eq. (9) and (10), respectively.

In this work, the calibrated FE model is referred to as the reference state, which corresponds to the structure's state when field tests were performed. Artificial damage scenarios were later introduced to the viaduct's longitudinal beams in this model to simulate crack formation and localized stiffness loss caused by exposure to operational loads, overloads, or accidents, a critical phenomenon to the structural arrangement's safety. Damage was incorporated into the model through equivalent cross-sectional reductions in Young's modulus (E), representing the physical degradation of flexural stiffness associated with crack openings (Figure 4). This approach is analogous to the reduction in a beam's effective height due to crack depth, where the E reduction proportionally simulates the loss in load-bearing capacity caused by effective height reduction. As demonstrated in [1, 28, 29, 88, 89], this penalization method induces measurable changes in mode shapes, which can be captured by modal curvature analysis, effectively localizing stiffness loss and representing damage presence. Seven damage intensities (5%, 10%, 15%, 20%, 25%, 30%, and 35%) were applied to the equivalent sections by reducing the modulus of elasticity. This reduction physically simulates the structural impact of cracks, analogous to a decrease in the beam's effective height due to crack depths of up to 20 cm. For each predefined crack depth (20 cm), 160 unique damage scenarios, representing variations in crack location or configuration, were generated. By applying all seven damage intensities to these 160 scenarios, a total of 1120 cases were incorporated into the database for each longitudinal girder.

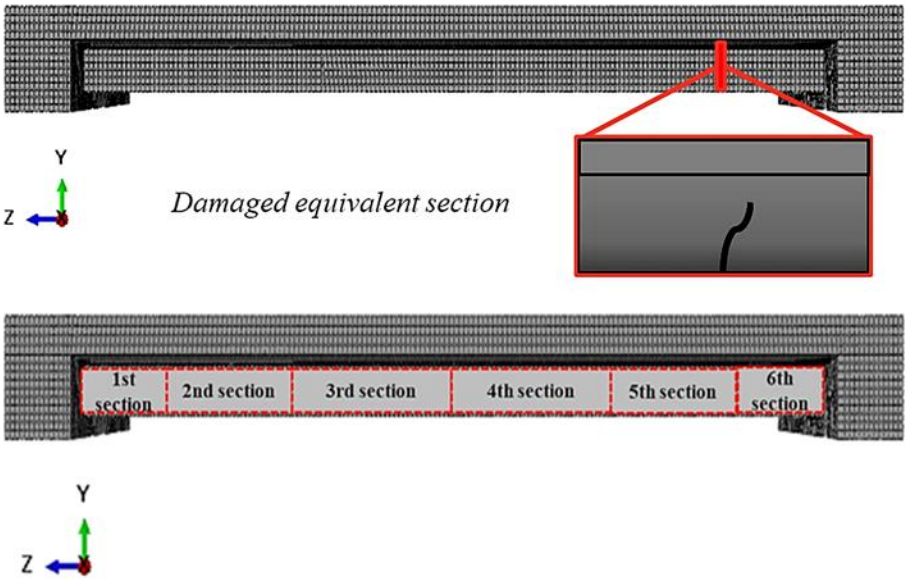

Figure 4 - Equivalent damaged section

4.3.
Damage indicator selection

Some dynamic structural features can be used as indicators of the presence and extent of damage [90, 91]. The data provided must be clean of environmental and noise effects, which always limits the use of primary dynamic properties, such as natural frequencies and mode shapes. To overcome this problem, dynamic indices have emerged, which use these properties to generate filtered secondary data useful for damage assessment.

The methodology proposed in this work relies in at least a pair of indices to prevent that peculiarities associated with a certain index create noise in the database. In this study, the selected indices were Modal Curvature Method (MCM) and the Modal Strain Energy (MSE) method. Their selection was based on findings from previous researchers. According to Fan and Qiao [91], the MCM is not sensitive to local damage caused by changes in the vibration shapes with low frequencies and has demonstrated satisfactory robustness in the presence noise. Tan *et al.* [88] report that the MSE method uses changes in the modal strain energy to detect damage in structures and is suitable for investigating scenarios with potential multiple damages. The choice of using a modal shape byproduct as input for the neural networks was supported by the representativeness of the experimental grid from the test, even with its limited duration, and by previous studies [29, 92, 93] that demonstrated the lower sensitivity of modal shapes to environmental variations compared to natural frequencies. According to Equations

7 to 10, the damage indicators are calculated from the sum of modal displacements of vibration modes. Thus, a Linear Perturbation set with Frequency analysis in Abaqus is indicated to obtain the necessary data. The Abaqus Analysis User's Guide [94] confirms that this approach accurately captures fundamental dynamic characteristics for vibration problems.

For the training and testing of an ANN, it is necessary to create a representative and reliable database. Introducing damage to a structure in service would be unsafe and pose risks to its users. This is one of the reasons why many authors introduce artificial damage in a calibrated finite element model [1, 25, 89, 95]. Another and more important reason for using this approach is that it enables the simulation of different damage scenarios, which would be difficult, if not impossible, to do in the physical structure. This is because once damage is introduced in the physical structure, it cannot be totally undone. Furthermore, to create a reliable database many damage scenarios are necessary, which can only be achieved through the introduction of artificial damage in the model.

The structural condition diagnosis is performed in two sequential stages, using multilayer perceptron artificial neural networks. In the first stage, a classifier neural network analyzes the structure and identifies the presence of damage, locating it in one of six predefined sections of the longitudinal beams. If damage is detected, the process advances to the second stage, where a regressive neural network estimates the severity of the damage identified in the previous stage.

5.
Proposed Framework

The pre-DT workflow for infrastructure management integrates multi-source data through a systematic process (Figure 5). Initially, an infrastructure asset is selected, and comprehensive data, including design specifications (structural plans and material details) and field measurements (ambient vibration tests), are aggregated into a digital asset inventory. This centralized repository supports three critical analytical models: a Finite Element (FE) for structural analysis, Artificial Neural Networks (ANNs) for structure condition assessment, and a Building Information Modeling (BIM) for comprehensive representation and data storage. These components collectively contribute to the creation of the pre-DT, which provides a dynamic and data-driven representation of the infrastructure. Finally, asset management utilizes DT for decision-making, monitoring, and maintenance planning, ensuring the optimal performance and safety of the structure. Additionally, a feedback loop from pre-DT to the asset inventory allows continuous updates based on new data and insights.

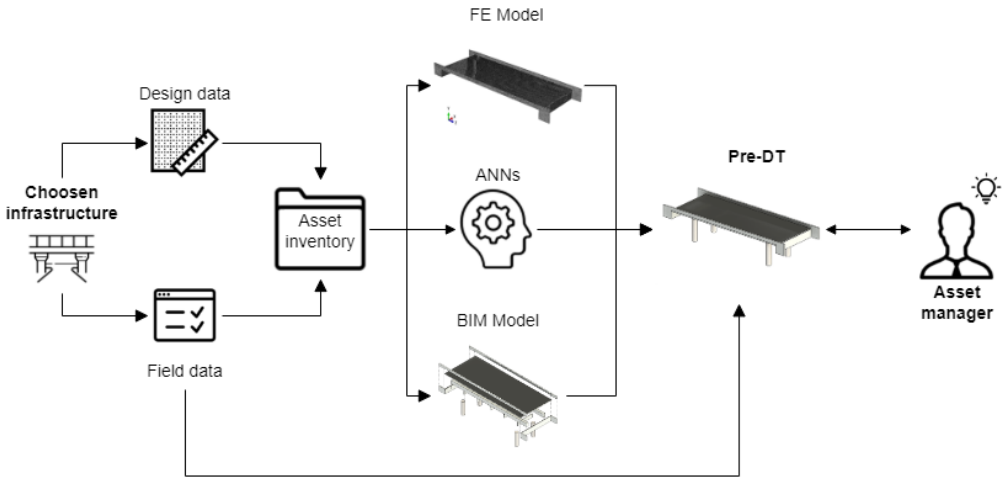

Figure 5 - Complete framework overview

The process involves four key stakeholders: Asset Management Team, Engineering Team, Modeling Team, and Data Science Team. The Asset Management Team initiates the process by selecting the assets to be monitored and determining maintenance interventions based on their condition. The Engineering Team, which includes experimentalists and structural specialists, conducts field tests, verifies design information, and generates periodic inspection reports to enhance the Digital Twin (DT). The Modeling Team, composed of experts

in numerical and information modeling, oversees the digital transformation by managing asset data requests, developing the BIM and FE models, and refining predictive state models to build the Digital Twin. Lastly, the Data Science Team is responsible for establishing databases and training artificial neural networks (ANNs) to validate and improve predictive analytics, supporting the data-driven decision-making.

The process of pre-DT implementation (Figure 6) begins with the Asset Manager defining the target infrastructure. Subsequently, the Modeling Team creates a comprehensive document for the Engineering Team, outlining all necessary information to construct the structure's virtual models. This document specifies: verified actual and design measurements, dynamic test-derived modal properties, the structural elements to be analyzed, and their physical properties. Guided by this scope, the Engineering Team plans and conducts field tests, determining the appropriate test types and experimental mesh. Upon completion, they provide the Modeling Team with critical data, including natural frequency values, vibration modes, and element compressive strengths. The Modeling Team then uses this data to calibrate the structure’s finite element models and Building Information Model (BIM). With the calibrated finite element model, the Modeling Team generates simulated damage scenario results, which they deliver to the Data Science Team. These results are used to build databases for training and validating Artificial Neural Networks (ANNs) that will diagnose structural health. Finally, the Digital Twin is consolidated by integrating these tools into the BIM model. The Engineering Team leverages the Digital Twin to generate detailed reports that assist the Asset Manager in making informed decisions regarding potential interventions. Crucially, the Engineering Team documents all real-world interventions and shares this information with the Modeling Team to ensure the Digital Twin remains up-to-date. This iterative process creates a continuous feedback loop, ensuring the Digital Twin accurately reflects the asset's current state and enabling informed management decisions.

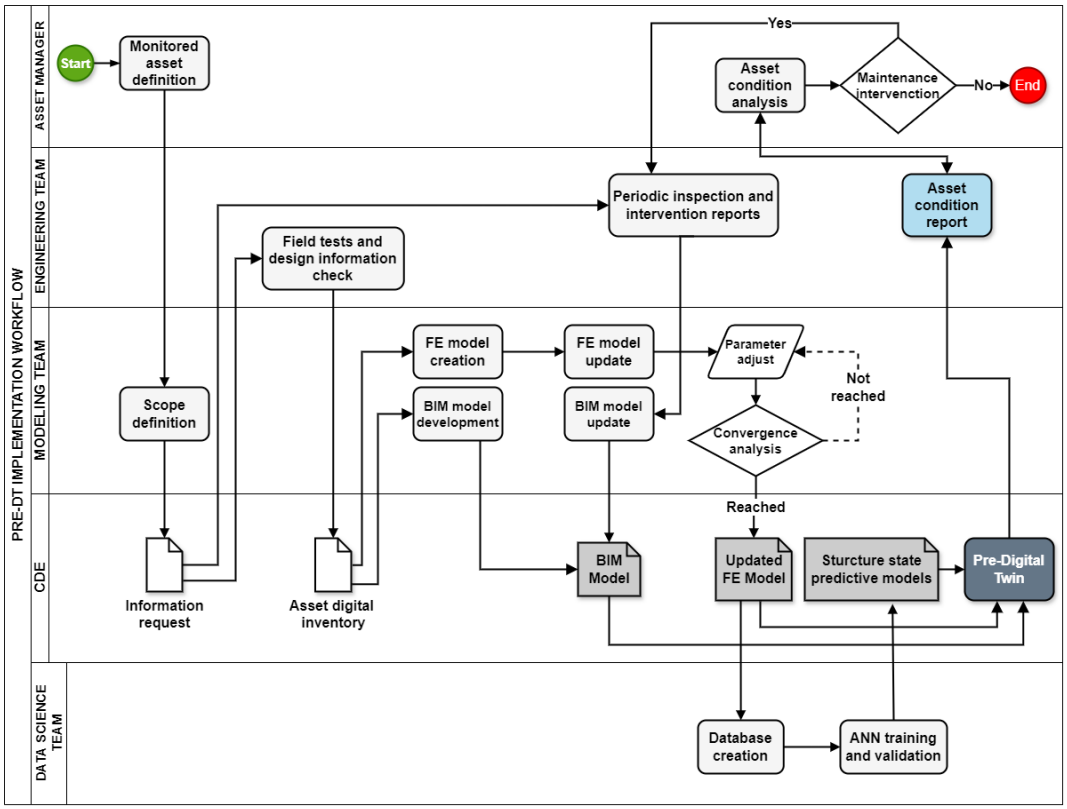

Figure 6 - Process map

5.1.

Digital inventory

The asset's digital inventory aims to create a comprehensive repository of data and attributes. Its primary goal is to facilitate continuous monitoring and efficient management of the asset's condition by providing a thorough the understanding of its state, therefore supporting proactive maintenance strategies. The process begins with the development of a 3D as-is BIM model based on design drawings, where critical attributes and relevant data are integrated. This inventory is organized as a database, consolidating all necessary information to enhance the efficiency of bridge management. The inventory includes general data and detailed information on design parameters, structural data, maintenance records, and structural condition diagnosis as shown in Figure 7. By serving as a centralized and structured repository, the inventory is intended to support effective management and informed decision-making for bridge maintenance and inspections.

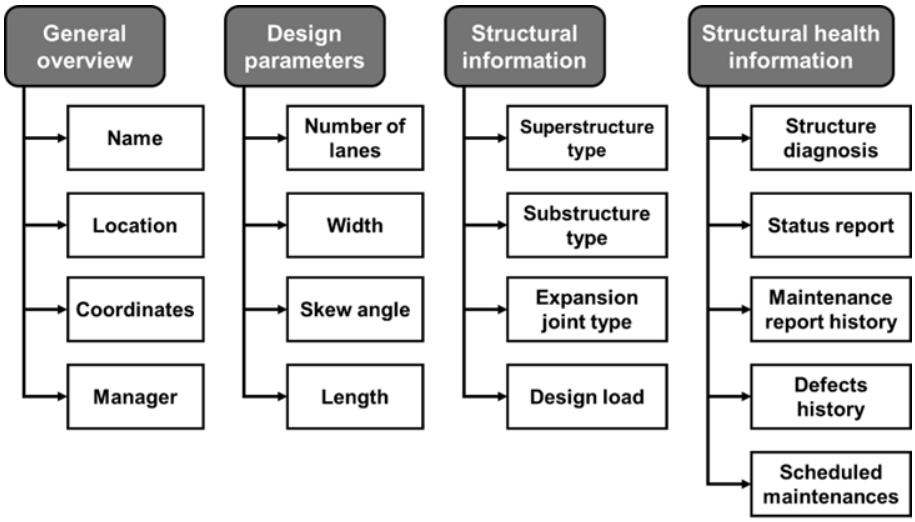

Figure 7 – Asset's inventory content

5.2.
Field tests

The field tests contribute to filling the structure's digital inventory. This data can be divided into two categories: structural behavior and structural component properties. Regarding structural behavior, the tests provide information on how the structure responds to external excitation, such as loads or wind effects. The choice of structural behavior tests in practice depends on the availability of traffic interruption (Figure 8). Ambient vibration tests, which can be conducted during the structure's operation, enables the determination of natural frequencies, vibration modes, and damping ratio. In contrast, static load tests, which can require traffic interruption, provides information on the stiffness of the structural elements and the structure's boundary conditions. The materials tests provide information on the structural element's strength. This data provides a stiffness estimate, which influences dynamic behavior and updating process of the numerical model.

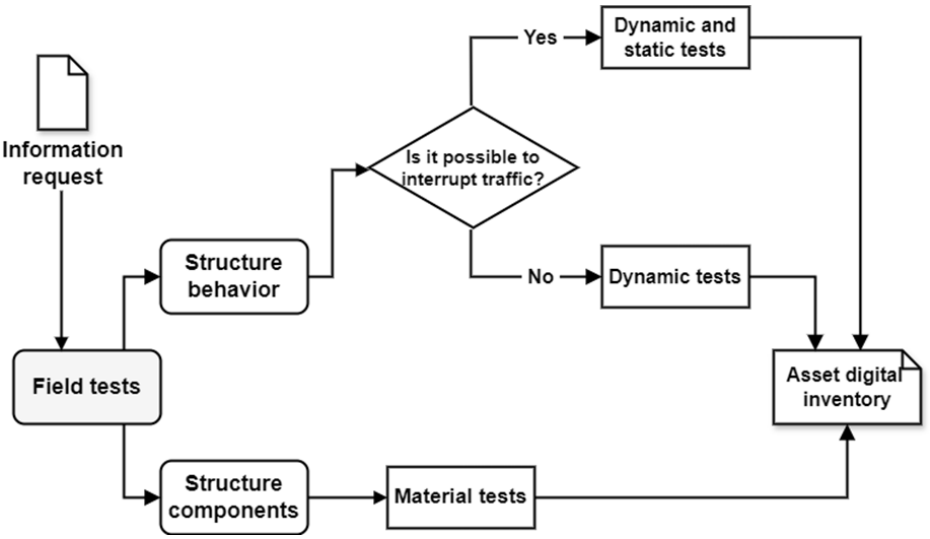

Figure 8 - Field tests framework

5.3.
FEM model creation

By the end of the updating stage, the finite element model should accurately reflect the structure's behavior as measured in the tests. Adjusting the model based on the results of the ambient vibration test requires assessing the similarity between the experimental and numerical results in terms of natural frequencies and vibration modes. The majority of the calibration effort focuses on the model's mass and stiffness, since these are the two main variables in the dynamic problem. In this work, the mass was adjusted by varying the asphalt layer´s thickness, while the stiffness calibrated by changing the Young's modulus of the structure´s material.

5.4.
ANNs for damage diagnosis

Artificial Neural Networks (ANNs) must be trained with a dataset of damage indicators to assess a structure's condition accurately. To ensure reliable results, the training data must be free from noise and interference caused by environmental factors such as temperature variations and wind. In this context, dynamic indices provide a more robust alternative to primary variables like natural frequency and vibration modes, as they are less sensitive to noise and environmental fluctuations. This enhances the accuracy of damage detection and quantification. The dataset is generated by introducing artificial damage scenarios into a calibrated finite element model. Using a finite element model for these analyses, rather than applying physical damage to the actual structure, is necessary due to the

operational challenges of accessing specific damage locations and the risks associated with modifying a structure that remains in service. Artificial damage is simulated by reducing the bending stiffness (EI) in designated sections of the longitudinal beams.

In this work the modal curvature index is adopted as the input variable for the ANNs. This choice is justified because the proposed methodology is based on sparse field tests rather than having to rely on continuous monitoring of the structure, which would require filtering out environmental effects using statistical methods. Fan and Qiao [91] note that the MCM is not sensitive to local damage caused by low-frequency changes in vibration shapes and has demonstrated satisfactory robustness in the presence of noise. Using a modal shape byproduct as input for the neural networks is further supported by the representativeness of the experimental grid, even with its limited duration, and by previous studies [29, 92, 93] that have shown modal shapes to be less sensitive to environmental variations compared to natural frequencies. According to eq. 7 and 10, the damage indicators are calculated from the sum of modal displacements across vibration modes. A Linear Perturbation Frequency analysis in Abaqus is conducted to extract the system's dynamic data. According to the Abaqus Analysis User's Guide [94], this method is able to find the fundamental dynamic properties relevant to vibration. In this analysis, the response is assumed linear and sufficiently small, so the system's inherent dynamic behavior is captured without accounting for history-dependent effects. This step can be executed independently of prior processes, and its solution provides eigenvalues (natural frequencies) and eigenvectors (mode shapes), which are essential for evaluating dynamic performance.

5.5. BIM-SHM integration

The integration proposed in this work occurs on three fronts: general overview, asset inventory, and structural diagnosis. In the first one, a tool is used to display a web dashboard that consolidates reports from all the concessionaire's assets, including information about the location of bridges and viaducts, the main pathologies found, and a ranking that orders these structures according to the criticality degree of their deterioration. Figure 9 describes in detail the general structure of this plugin component. To populate the dashboard, asset condition reports are initially obtained, and stored in the Common Data Environment (CDE). Then, these reports update a Power BI dashboard, which is published on the web, facilitating access to information. In parallel, a script integrated with the BIM tool

interacts with the CDE and the online publication, ensuring data visualization and monitoring.

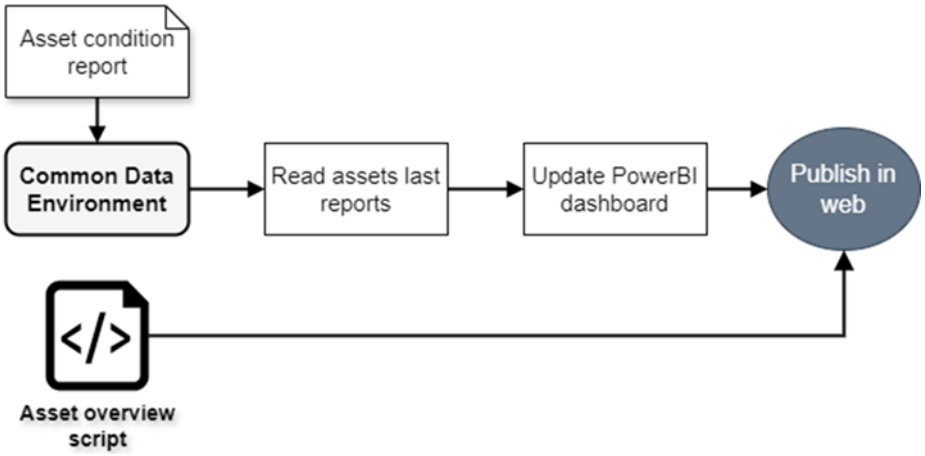

Figure 9 - Assets overview code framework

The viaduct inventory is divided into two parts: static and inspection data. The static part gathers information that remains unchanged or undergoes few changes during the infrastructure's lifespan, allowing it to be organized in a fixed database, accessible through script. This section covers general, engineering, and structural data, as illustrated in Figure 10a, which details the operation of the code responsible for integrating them. This data, like all other structural data, is centralized in the Common Data Environment (CDE). Then, the script collects and organizes the information, converting it to a format compatible with the display on the BIM platform, and presents the result in a text window, enabling a clear and consolidated view of the inventory. Figure 10b shows the operation of the code that displays inspection information. This code generates a list of all available inspection reports, displayed in a selection window, where the user can choose a specific report to view. Upon selecting a report, the system opens a new window that shows the chosen report. This way, users can navigate and view different inspection reports on the BIM platform, facilitating the analysis and management of this information.

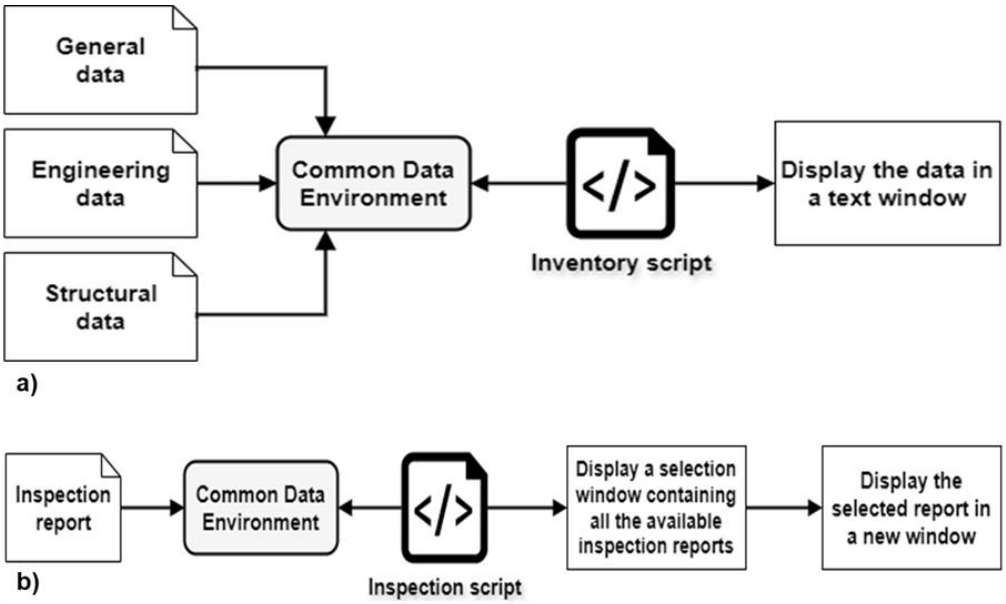

Figure 10 - Code framework for accessing and visualizing a) static and b) inspection data

The integration front concludes with a structural diagnosis, executed through three sequential scripts. As depicted in Figure 11a, the analysis script initiates the diagnostic workflow. First, it retrieves the most recent modal curvature data, captured during ambient vibration tests and stored in the Common Data Environment (CDE), and processes it using two pre-trained neural networks. The localization network detects the presence and location of structural damage. If damage is identified, the severity identification network evaluates its intensity. These results are compiled into a diagnostic report, which states whether damage exists, specifies the affected structural element, pinpoints its location, and quantifies its severity. Next, the incorporate function (Figure 11b) integrates this report into the digital structural model. Using shared parameters, the function updates longitudinal beam model groups by assigning two key properties to the relevant elements: damage existence and damage severity. These parameters are linked to specific structural members via their unique IDs, ensuring traceability. Finally, the results function (Figure 11c) generates an interactive 3D view that visually highlights elements requiring attention. This view dynamically adjusts element appearances based on their shared parameter values, applying filters to emphasize compromised areas. Accessible online, the visualization supplements the manager’s final report with actionable insights into structural health.

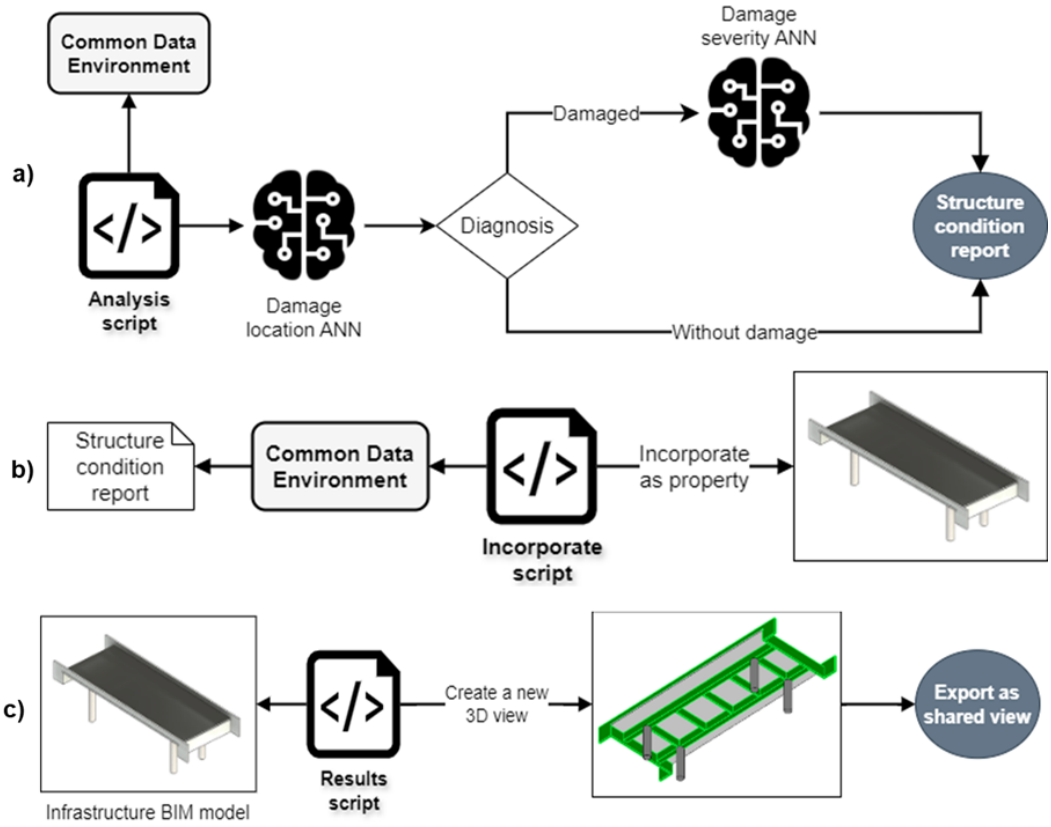

Figure 11 - Structure diagnosis code overview

The results related to the structural condition of the elements are integrated into the BIM model, enabling the generation of a report intended for the asset manager. This report displays all structural elements using a color-coded classification system that reflects the degree of degradation of each component. Structural conditions are categorized into four levels based on DNIT grading: undamaged (grade 5 - green), slightly deteriorated (grades 4 or 3 - yellow), highly deteriorated (grades 2 or 1 - purple), and potentially hazardous (grade 0 - red). Based on this report, which integrates SHM inspection data and the intervention history stored in the model, the manager can decide whether to carry out corrective maintenance, including it in the planned project schedule.

6.
Experimental program

6.1.
Case study

The Rio Claro-Viaduct is located in the city of Rio Claro, over the SP-340 highway. Situated in an urban area, the viaduct plays a crucial role in the region's infrastructure, serving as one of the main access routes to cities in the western part of the state of São Paulo, particularly connecting to São Carlos (Figure 12).

Figure 12 - Rio Claro-Viaduct

Constructed in the 1980s, this reinforced concrete viaduct boasts a robust structural design. It comprises two main girders, five transverse beams connecting them, and four supporting piers. Two bracing beams enhance the columns stability, while the deck provides the roadway surface. The structure terminates on both ends with wing walls that anchor it to the surrounding earth slopes. Spanning 32.1 meters in length and 13 meters in width, it traverses three spans and is laterally secured by New Jersey barriers (Figure 13).

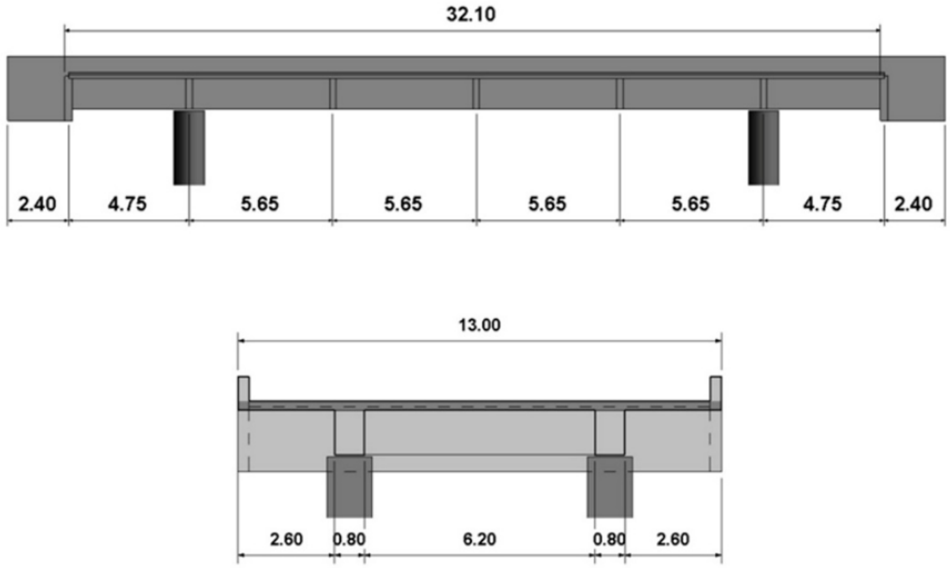

Figure 13 - Structure measurements (in meters)

Two key factors motivated the choice of this viaduct for the case study. First, researchers had access to dynamic measurements taken ten years apart, carried out by Gómez Araújo *et al.* [96] in 2014, enabling a thorough assessment of how the structure's behavior may have changed over this extended period. Second, since this viaduct shares design characteristics with numerous other bridges across Brazilian highways, the study's findings have broad applicability for evaluating similar infrastructure. The selection proved particularly valuable given the steady rise in traffic loads and the chance to examine structural deterioration across a meaningful timespan. The 2024 experimental campaign was carried out in collaboration with a research team from the São Carlos School of Engineering (USP), led by Professor Ricardo Carrazedo.

6.2.
Experimental setup

6.2.1.
Ambient vibration tests

Dynamic monitoring was performed in both tests using identical equipment configurations. Nine Brüel and Kjær uniaxial piezoelectric accelerometers were employed: five model 4533-B-002 (490 mV/g sensitivity, frequency range 0.2 Hz–12.8 kHz) and four model 8344 (2500 mV/g sensitivity, frequency range 0.2 Hz–3 kHz). These were connected via Brüel and Kjær AC-0005-N ultra-low noise cables to a National Instruments acquisition system, which included three NI 9232

modules (three channels each) housed in an NI cDAQ-9174 chassis, totaling nine channels. Signal acquisition was controlled using National Instruments' Signal Express software [97] on a laptop. Data was sampled at 984.62 Hz—the system's minimum supported sampling frequency—with each test lasting 20 minutes.

Vertical acceleration measurements were conducted at 30 different points on the structure, distributed along the pedestrian walkways. Figure 14 details the layout, highlighting the measurement points from the most recent ambient vibration test and the points recorded during the previous test conducted in 2014.

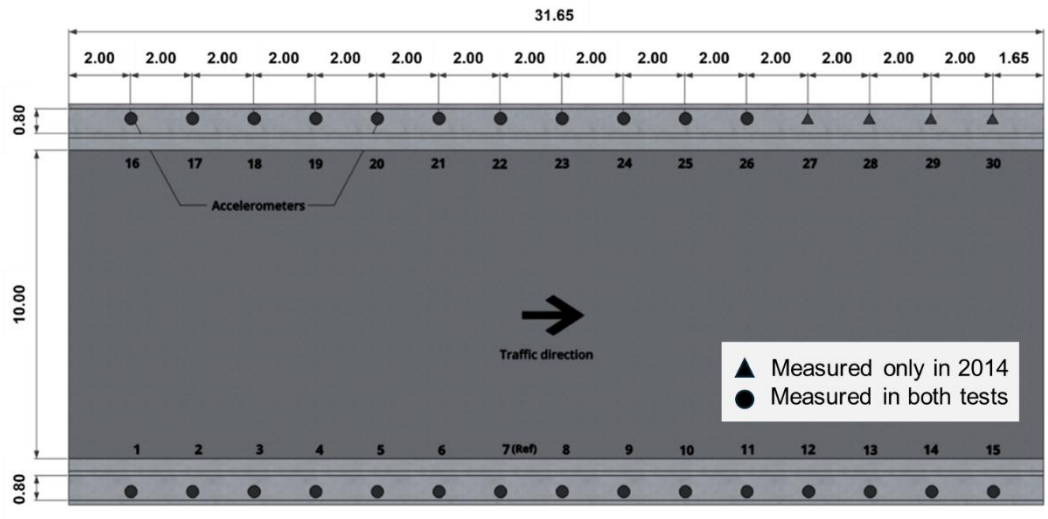

Figure 14 - Top view and detailed layout of the viaduct with measurement points (in meters)

Given that the number of measurement positions required for modal identification exceeded the number of available accelerometers, six different setups were necessary to cover all measurement points. A fixed reference point (7 ref) was chosen as common to all tests, while the other measurement positions were distributed according to Table 3. It is important to note that although points 13, 14, and 15 were measured during the most recent test, they did not satisfactorily capture vertical acceleration information and were excluded from the mode shape analysis. This failure in data acquisition could be attributed to several factors, including environmental conditions or equipment malfunctions.

Table 3 - Accelerometers setups distribution

Setup	Measurement points																									
	1	2	3	4	5	6	7	8	9	10	11	12	13	14	15	16	17	18	19	20	21	22	23	24	25	26
1	•			•			•	•		•				•												
2		•			•		•		•		•				•											
3			•			•	•					•	•													
4							•									•		•					•		•	
5							•										•		•					•		•
6							•													•	•	•				

Using the field data obtained, modal analysis was performed using two different techniques: EFDD, in the frequency domain and SSI-COV, in the time domain, both implemented in the ARTeMIS Modal [98].

6.2.2.
Material properties investigation

Characterizing the structure materials properties is another necessary aspect of preparing the viaduct model update. Concrete properties vary spatially in the structure due to factors like different concrete batches, curing conditions, or execution dates [99]. Maracchini *et al.* [100] emphasize that uncertainty in concrete strength, especially in key structural elements, is a determining factor for structural assessments and the correct representation of its physical behavior through a numerical model. Therefore, reliable data must be collected to support the selection of the properties of the modeling materials, going beyond the information contained in the design.

Non-destructive tests were employed to assess the viaduct's physical properties without disrupting its operation. A Schmidt HT-225 concrete test hammer (measurement range: 10–60 MPa) was used for the assessment. To obtain representative values, three experimental points (EPs) were selected within a defined mesh (Figure 15) for each longitudinal girder. These elements were identified as critical components of the structure, making them the primary focus of the material properties investigation. The compressive strength was then estimated as the average of the recorded readings. This information was incorporated into the numerical model as Young's Modulus (E) for the tested elements. The estimation of this value was calculated using Equation 10 from the Model code, which takes the following form:

$$E = E_{c0} \times \alpha_e \times \left(\frac{f_{cm}}{10}\right)^{1/3} \tag{11}$$

where $E_{c0} = 21.5\ GPa$, α_e is a coefficient to the aggregate quality and f_{cm} is the mean value of concrete compressive strength.

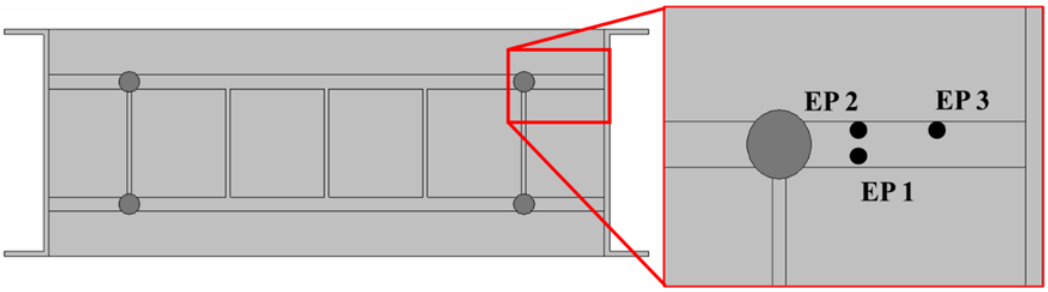

Figure 15 - Rebound hammer test experimental grid

6.2.3.

Support stiffness measurement

To characterize the viaduct support condition, a rectilinear displacement transducer, model GEFRAN PY2-C-025, was installed in the gap between the lower face of the longitudinal girder and the upper face of one of the columns (Figure 16). The transducer was attached to the structure using an L-shaped shelf and double-sided tape. Electrical signals generated from the vibrations caused by traffic were captured and transferred at a rate of 100 samples per second to an acquisition system.

During the acquisition period, the times when three-axle trucks were traveling directly above the monitored support were recorded. The weights of these vehicles were estimated based on the National Department of Transport Infrastructure (DNIT) traffic standards [101]. Subsequently, the corresponding displacements were verified and the results were used to estimate the elastic constant of the viaduct support, considering it as a linear spring.

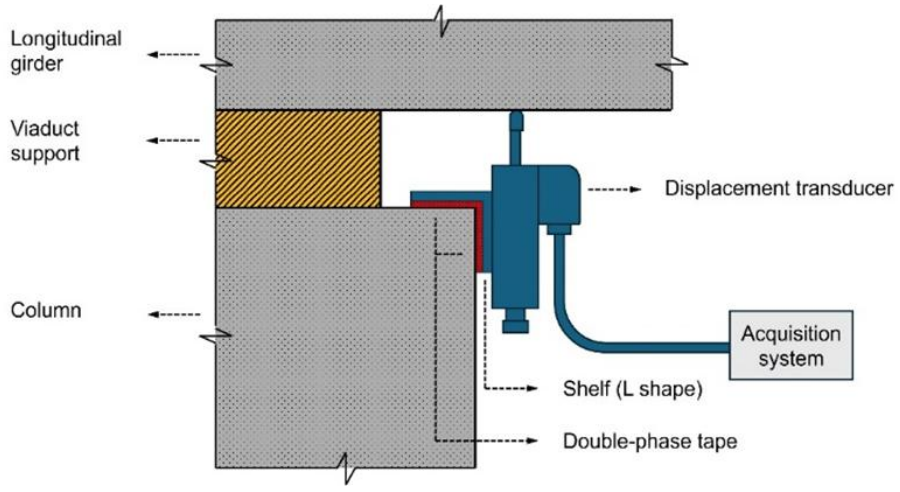

Figure 16 - Transducer installation scheme

6.3.
Modal properties

6.3.1.
Results from 2014 tests

The first modal tests performed on the case study viaduct were conducted in 2014 [96]. The original data includes vertical acceleration measurements recorded at 30 different points in a total of seven setups. Similar to the 2024 test, for each setup, the time series were collected for 20 minutes at a sampling frequency of 984.6 Hz. For the EFDD technique, the spectral densities were estimated with a resolution of 1024 and a frequency line spacing of 0.048 Hz. The natural frequencies of the viaduct were identified by locating the peaks in the singular value plots of the PSD matrix of all measurements, as shown in Figure 17a. Similarly, for the SSI method, the UPC merged estimator was selected and the frequencies were determined through the alignment of stable poles in the stabilization diagram (Figure 17b).

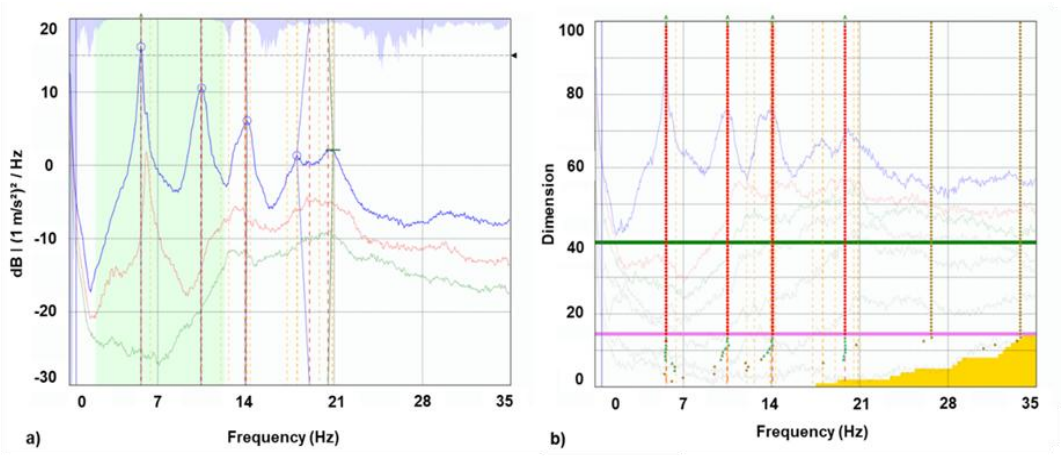

Figure 17 - (a) EFDD analysis and (b) SSI-COV analysis for all setups using the 2014 data

Finally, five natural frequencies and corresponding damping ratios were obtained using the EFDD method, while the SSI-COV method captured four modes, all of which were vertical bending modes. The identified modal parameters and their comparison are summarized in Table 4, and Figure 18 illustrates the corresponding mode shapes. The correlation between mode shapes from the two techniques was assessed using the MAC method, as shown in Figure 19.

Table 4 - Natural frequencies and damping ratios of the viaduct from 2014, identified using the EFDD and SSI-COV methods

Mode shape	EFDD (2014)		SSI-COV (2014)		Average	
	NF (Hz)	D (%)	NF (Hz)	D (%)	NF (Hz)	D (%)
1	5.68	2.28	5.63	3.35	5.65	2.82
2	10.42	3.95	10.51	6.52	10.46	5.24
3	13.96	2.85	14.08	4.85	14.02	3.85
4	19.04	2.21	19.28	6.22	19.16	4.21
5	20.51	2.19	#	#	20.51	2.19

Note: NF = Natural Frequency; D= Damping ratio; # = Undefined.

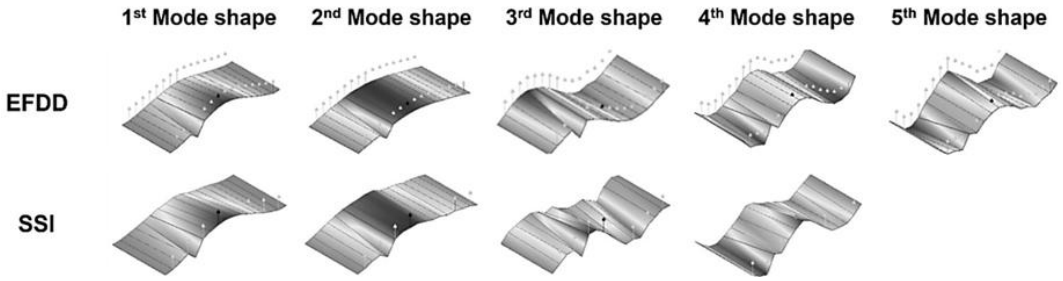

Figure 18 - Comparison of the mode shapes identified using EFDD and SSI through ARTeMIS from the 2014 vibration measurements

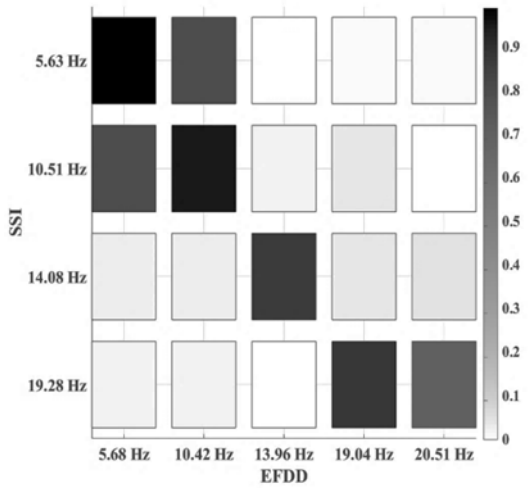

Figure 19 - MAC results for the two methods used in modal identification of 2014 data

The values in Table 5 show a strong correlation between the two methods in terms of natural frequencies, with discrepancies of 1% or less. Additionally, the MAC results in Figure 19 show mode shape correspondences exceeding 0.8, indicating a good correlation between the vibration modes. This observation can also be graphically demonstrated in Figure 19, where the diagonal elements exhibit values close to unity. The off-diagonal results indicate a similarity between the shapes of the first and second vibration modes. However, the 4.79 Hz difference between their natural frequencies confirms that they are distinct modes. The last

two vibration modes identified by EFDD (19.04 Hz and 20.51 Hz) showed shapes similar to the last mode obtained by SSI (19.28 Hz). The 19.04 Hz mode stood out due to its closer proximity to the ideal correlation (MAC of 0.88), while the 20.51 Hz mode presented a MAC of 0.71. The damping ratios identified range from 2.82% to 5.24% on average, considering only the modes captured by both methods. Typically, damping ratios from ambient vibration tests of full-scale bridges reported in the literature [102] do not exceed 2-3%, while reinforced concrete bridges are traditionally assumed to have a 5% damping ratio across all vibration modes [103]. Therefore, the identified values fall within a reasonable and expected range.

6.3.2.
Results from 2024 tests

For the recent dynamic test, conducted approximately ten years after the initial one, the same methodology was applied to process the data. Fig. 20a highlights the selected peaks in the singular value plots corresponding to potential natural frequencies, while Fig. 20b presents the stabilization diagram generated by the SSI-COV algorithm.

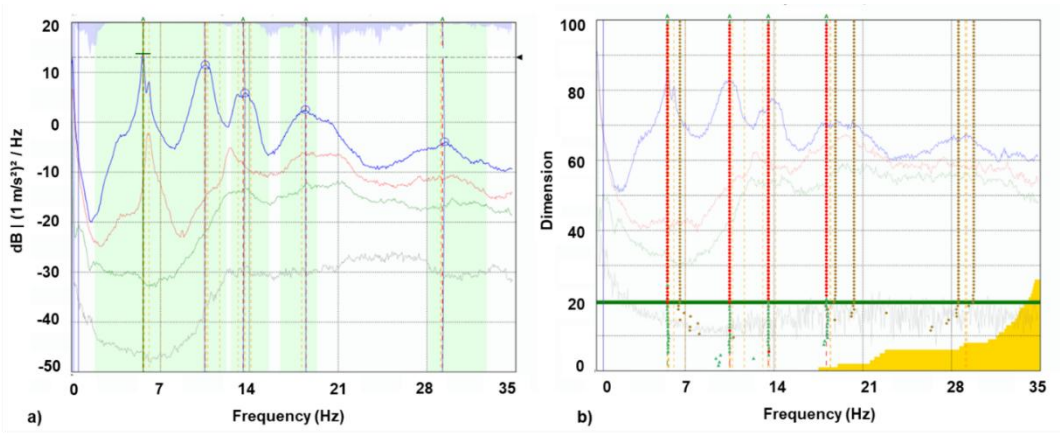

Figure 20 - (a) EFDD analysis and (b) SSI-COV analysis for all setups using the 2024 data

Similarly, modal identification using the EFDD method identified five vibration modes, while the SSI-COV method captured four, all of which were vertical bending modes (Fig. 21). The summarized modal information is presented in Table 5.

Table 5 - Natural frequencies and damping ratios of the viaduct from 2024, identified using the EFDD and SSI-COV methods

Mode shape	EFDD (2024)		SSI-COV (2024)		Average	
	NF (Hz)	D (%)	NF (Hz)	D (%)	NF (Hz)	D (%)
1	5.63	3.96	5.59	4.86	5.61	4.41
2	10.48	4.78	10.49	3.36	10.49	4.07
3	13.51	3.48	13.55	2.18	13.53	2.83
4	18.46	2.52	18.13	4.83	18.30	3.67
5	29.22	2.01	#	#	29.22	2.01

Note: NF = Natural Frequency; D= Damping ratio; # = Undefined.

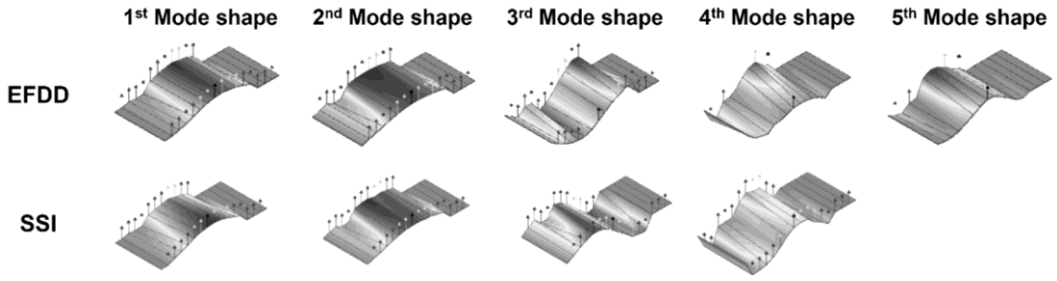

Figure 21 - Comparison of the mode shapes identified using EFDD and SSI through ARTeMIS from the 2024 vibration measurements

As shown in Table 4, the differences between the natural frequencies identified by the various methods are minimal, generally 1% or less, similar to the 2014 modal data. The MAC values plotted in Figure 22 indicate a high degree of similarity between the first and second mode shapes, and values close to unity for the first three frequencies on the diagonal, indicating again strong correspondence between the mode shapes captured by different methods. This alignment is further illustrated in Figure 19, which also demonstrates that the unmeasured points influenced the deformation patterns of the viaduct at each associated frequency.

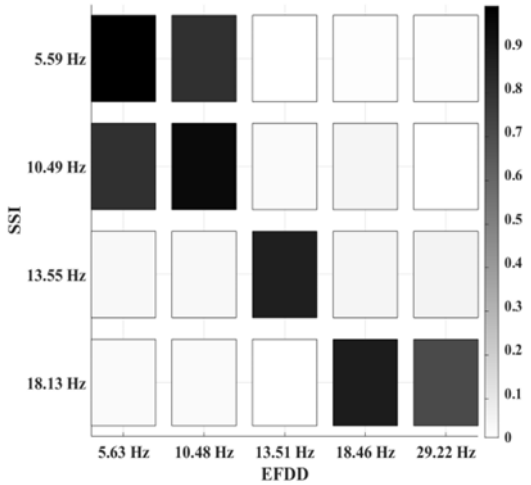

Figure 22 - MAC results for the two methods used in modal identification of 2024 data

6.3.3.
2014 and 2024 results comparison

As stated in a previous section, the first comparative analysis conducted in this study involved comparing the modal parameters obtained from the post-processing of the 2014 monitoring data with those reported by Gómez Araujo *et al.* [96], where the authors employed an approach called Enhanced Power Spectral Density Transmissibility Matrix with Singular Value Decomposition (E-PSDTM-SVD). This comparison was essential for validating the reanalysis and ensuring methodological consistency. The correlation between mode shapes was assessed through frequency discrepancies, represented as Δ in the last two rows of Table 6.

Table 6 - Comparison of the results delivered by EFDD and SSI-COV methods with those reported by Gómez Araújo et al. [96] using the E-PSDTM-SVD method

Mode shape	EFDD (2014)		SSI-COV (2014)		E-PSDTM-SDV		$\Delta_{EFDD/E-PSDTM}$	$\Delta_{SSI/E-PSDTM}$
	NF (Hz)	D (%)	NF (Hz)	D (%)	NF (Hz)	D (%)		
1	5.68	2.28	5.63	3.35	5.65	2.89	0.53	-0.35
2	#	#	#	#	7.35	0.71	#	#
3	10.42	3.95	10.51	6.52	10.41	2.47	0.10	0.96
4	#	#	#	#	12.87	2	#	#
5	13.96	2.85	14.08	4.85	13.96	2.19	0.00	0.86
6	19.04	2.21	19.28	6.22	17.59	1.92	8.24	9.60
7	20.51	2.19	#	#	21.39	1.92	-4.11	#

Note: NF = Natural Frequency; D= Damping ratio; # = Undefined.

Based on the data in Table 6, it is evident that the E-PSDTM-SVD method identified significantly more closely spaced vibration modes. Despite this, the comparison of the first three similar modes shows a percentage difference of less than 1%, indicating good agreement between the methods, although higher frequency values exhibit discrepancies. Inspection of Figure 23 reveals the similarity between the matched mode shapes.

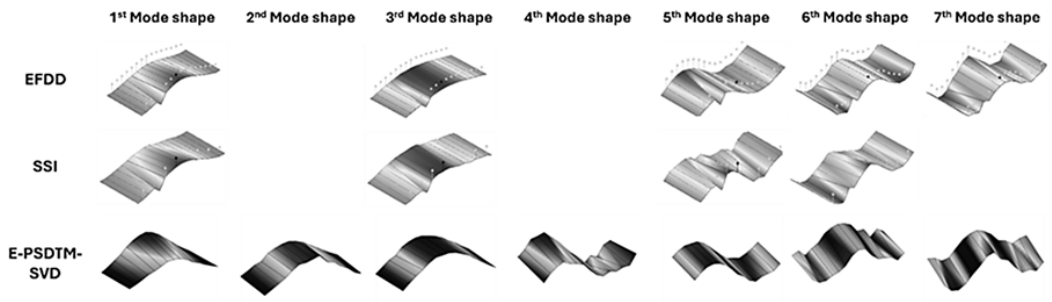

Figure 23 - Mode shapes from 2014 test obtained using different methods

Table 7 presents the natural frequency and damping factor values obtained by the EFDD and SSI-COV methods for the dynamic monitoring conducted in 2014

and 2024. The delta value in the last column represents the percentage difference between the average values obtained in the older test and the average from the more recent test. Positive values indicate a decrease in frequency, which is expected, as increased damage typically leads to a reduction in structural stiffness. This behavior is also reported in bridge studies referenced by Doebling *et al.* [104]. However, the frequency changes observed fall within the range of -0.2% to 4.5%, which is not significant enough to suggest any substantial damage to the structure. This shift in modal frequencies could be associated with operational service or even environmental conditions as highlighted by Cremona [105].

Table 7 - Comparison between the modal parameters estimated in the two tests (2014 and 2024)

Mode	EFDD (2014)		SSI-COV (2014)		E-PSDTM-SDV		E-PSDTM-SDV		Δ (%)
shape	NF (Hz)	D (%)	NF (Hz)	D (%)	NF (Hz)	D (%)	NF (Hz)	D (%)	
1	5.68	2.28	5.63	3.35	5.63	3.96	5.59	4.86	0.8
2	10.42	3.95	10.51	6.52	10.48	4.78	10.49	3.36	-0.2
3	13.96	2.85	14.08	4.85	13.51	3.48	13.55	2.18	3.5
4	19.04	2.21	19.28	6.22	18.46	2.52	18.13	4.83	4.5
5	20.51	2.19	#	#	#	#	#	#	#
6	#	#	#	#	29.22	2.01	#	#	#

Note: NF = Natural Frequency; D= Damping ratio; # = Undefined.

The damping ratios identified in both experimental campaigns (Table 7) remained stable over the 10-year period, averaging 3.1–4.9% in 2024 compared to 2.8–5.2% in 2014. While recent studies highlight challenges in damping estimation due to factors like signal non-stationarity and environmental variability [106], the consistency observed here, under repeated tests with controlled setups, aligns with literature indicating that stable damping ratios in reinforced concrete structures correlate with structural integrity [103]. This stability, coupled with minimal frequency shifts (≤4.5%), reinforces the conclusion that no critical deterioration has occurred in the 10-year period.

The results from Tables 6 and 7 demonstrate the effectiveness of the proposed methodology, supported by three pillars: the analysis of natural frequency stability, redundancy in post-processing, and the adoption of a robust experimental mesh. Over 10 years, the observed frequency variations were limited to ≤4.5%, strongly contrasting with the 18% reported by Peeters [22] and the 15% found by De Angelis [44], recorded in shorter periods, even under conditions of greater ambient temperature amplitude. The reliability of the current method is partly attributed to the redundancy layer in post-processing, which applies EFDD and SSI analyses to validate the findings. Furthermore, the experimental mesh with 30 points on a 32.1m structure allowed for superior mode shape detailing,

surpassing setups in other studies which adopted only 8 points (58m) [22] and 26 points (120m) [44], which, despite being applied to larger structures, presented less dense spatial coverage. The observed stability, redundancy, and high experimental resolution confirm both the robustness of the approach and the consistency of the natural frequency and modal shape results.

6.4. Material investigation results

Tests to estimate the compressive strength of concrete in the structural elements revealed a heterogeneous material behavior. Using the rebound hammer in an upward vertical position, three readings were taken at each experimental point on each girder (Table 8). The left and right longitudinal girders showed compressive strengths of 39.7 MPa and 45.0 MPa, respectively. These differences were also reflected in the elastic moduli, which were incorporated into the model. Calculated using eq. 11, the elastic modulus values were 34 GPa and 35.5 GPa for the left and right girders, respectively.

Table 8 - Rebound hammer readings

Longitudinal girder	Experimental point	Readings			Standard
Left	E1	55	45	48	49.3
	E2	47	46	46	46.3
	E3	46	46	51	47.7
Right	E1	49	50	54	51.0
	E2	50	49	46	48.3
	E3	49	52	43	48.0

6.5. Support stiffness estimation

It was observed that near the monitored viaduct, there is a toll station operated by the road concessionaire responsible for controlling the flow of trucks traveling on this highway. Given that the truck weights comply with the guidelines of Brazilian traffic control institutions, a quasi-static approach was chosen to characterize the viaduct support.

During the displacement data acquisition period, the times when three-axle trucks passed directly above the monitored support were recorded. The estimated weight of these trucks is 24 tons, in accordance with DNIT [101]. By correlating this weight with the displacement data collected at these moments and considering that

the support behaves approximately like a linear spring, it was possible to estimate a spring stiffness of $7.2 \times 10^8 \ \ N/m$. This estimated value was, thus, used to obtain the responses of the numerical models discussed later in this section.

6.6. Partial conclusions

The data post-processing was expanded to compare key modal parameters using two distinct dynamic characterization techniques. Based on these results, it can be concluded that:

- The reanalysis of 2014 AVT data using the time-domain algorithm (SSI) ensures the previously obtained results. The natural frequencies in both cases showed a difference of 1% or less. The similarity between the compared vibration modes was demonstrated by MAC values, which compare the modal shapes captured in the situ for each natural frequency, with values of 0.8 or higher.
- The behavior observed in the 2014 test results was also seen in the 2024 results. The first four natural frequency values obtained by EFDD and SSI showed a difference of 2% or less. The MAC values were in a range of 0.8 or higher, indicating high similarity. These findings reinforce the robustness of the experimental data from both tests, as they were nearly identical when examined in both the time and frequency domains.
- There is a small difference between the natural frequency values observed in 2014 and 2024, indicating that the structural health condition has been maintained over this interval. The first two natural frequencies showed the smallest changes (<1%), while the others two showed a larger difference (≤4%). This observation can be attributed to the greater susceptibility of these vibration modes to environmental conditions or captured noise effects, without impacting the structural integrity diagnosis.
- The results presented in Table 5 confirmed the robustness and critical redundancy of the methodology proposed in this work. Post-processing with EFDD and SSI analyses ensured redundancy in data validation, while the use of a dense experimental mesh (30 points over a 32.1m span) guaranteed comprehensive coverage of the structure. These factors helped validate the reliability of the captured natural frequencies, which varied by 4.5% or less in 10 years, as well as the mode shapes, used in the numerical model adjustment.

7.
Numerical modeling

7.1.
Modeling strategy

In the initial stage of the numerical modeling, the three model proposed modeling strategies presented in section 4.2 were adjusted in five steps. Then, their natural frequencies and vibration modes were compared with the experimental results. Based on this comparison, one of the models was selected and refined in greater detail as is described in the next section. The absolute percentage error between the natural frequencies obtained by the physical test and the numerical model of the first four Mode Shapes (MS) are presented by the vertical axes of the graphs in Figures 24 to 26. The horizontal axis represents its evolution at each stage of the model adjustment. The first update step involves the initial configuration, based on project-collected information. The wings and abutment at the ends were added to the model in the second stage. From the third to the fourth step, the boundary conditions at the abutments were modified, starting from a simply supported configuration to a completely restricted. The last stage of model adjustment consisted of changing the concrete elasticity modulus (E). It should be noted that in models A and B (Figures 24 and 25), the increase in stiffness was not sufficient for the first natural frequency to reach values close to those observed in environmental vibration tests. In addition to showing natural frequency values closer to those observed by the physical structure, model C proved to be less sensitive to changes imposed during the updating stages (Figure 26). Even with less impact on the model's natural frequencies, the elasticity modulus adjustment proved its relevance in refining the results.

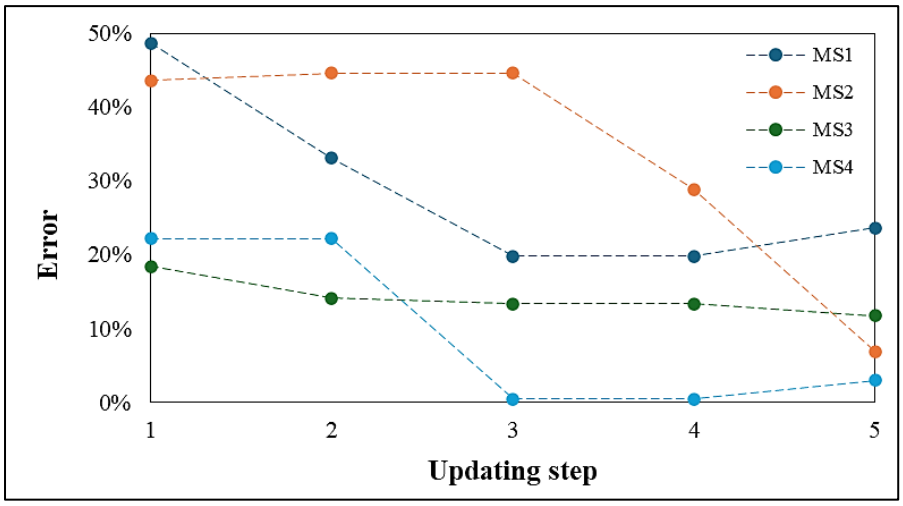

Figure 24 - Model A updating progress

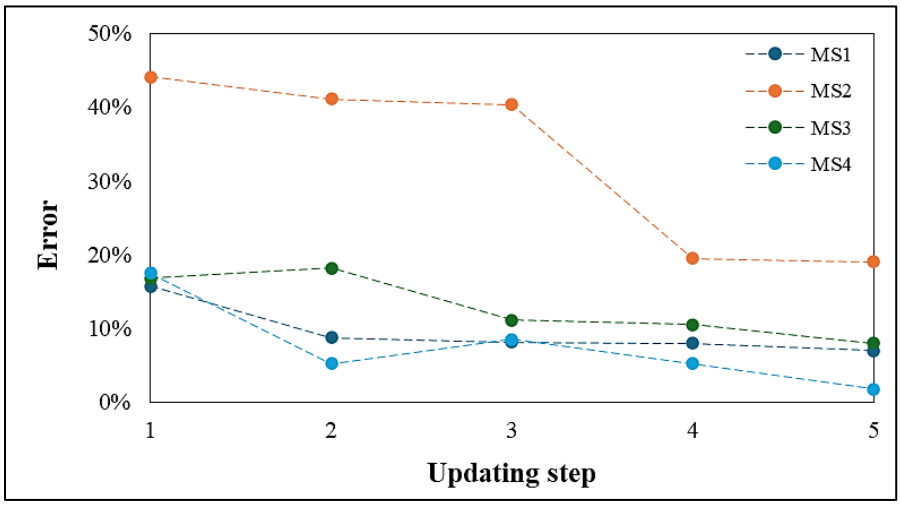

Figure 25 - Model B updating progress

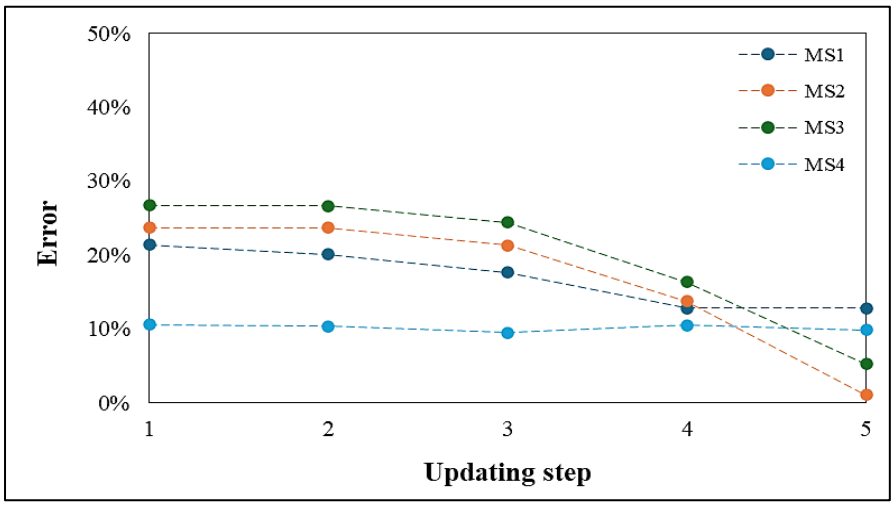

Figure 26 - Model C updating progress

Table 9 shows the difference between the initial and final natural frequencies after model calibration for each model. The most significant differences in absolute values could be noted in model A, which is initially more flexible than the others.

Table 9 - Natural frequencies comparison after FE model updating

Mode	Model A			Model B			Model C		
shape	Initial (Hz)	Final (Hz)	|Δ|	Initial (Hz)	Final (Hz)	|Δ|	Initial (Hz)	Final (Hz)	|Δ|
1	2.90	4.53	36%	6.19	5.32	16%	7.12	6.42	10%
2	7.26	12.07	40%	9.12	10.93	17%	16.90	13.04	23%
3	11.39	15.78	28%	17.06	12.99	31%	19.26	14.90	23%
4	21.49	17.65	22%	18.56	17.87	4%	20.33	20.17	1%

In Table 10 the values of the absolute errors between the natural frequencies obtained experimentally and numerically are shown. It is noted that model A reached distant values for the first and third vibration modes. Models B and C achieved closer numbers when compared to those captured experimentally, with a small advantage for C in modes 2 and 3.

Table 10 - Comparison between experimental and numerical natural frequencies

Natural	Model A		Model B		Model C	
Frequency	Final (Hz)	| Error|	Final (Hz)	| Error|	Final (Hz)	| Error|
5.59	4.53	19%	5.32	5%	6.42	15%
12.49	12.07	3%	10.93	12%	13.04	2%
13.55	15.78	12%	12.99	8%	14.90	6%
18.13	21.49	19%	17.87	1%	20.17	11%

The second criterion adopted to evaluate the model calibration was the MAC. The results demonstrated the similarity between the experimental and numerical vibration modes for most of the compared shapes (Table 11). Model C provides the best match between numerical and experimental mode shapes, with MAC values above 0.90 for all modes. Model B also performs well but has slightly lower correlations, particularly for the third mode (0.80). Model A shows good agreement for the first three modes but a weaker correlation for the fourth (0.65). The low values outside the main diagonal for all models confirm that each mode shape is unique. Although Model C showed only a slight advantage over Model B in terms of natural frequencies difference, the decision to adopt it for database creation was based on the analysis of modal curvature method. Considering that the MCM, used in predictive models, is sensitive to the vibration mode shape, Model C was chosen as it exhibited the highest correlation with experimental data, as indicated by the higher MAC values.

Table 11 - MAC and NF results

	Model A				Model B				Model C			
$MS1_{num}$	**0.97**	0.01	0.00	0.09	**0.93**	0.00	0.10	0.06	**0.96**	0.01	0.11	0.15
$MS2_{num}$	0.00	**0.93**	0.00	0.01	0.00	**0.89**	0.27	0.13	0.03	**0.93**	0.21	0.10
$MS3_{num}$	0.00	0.00	**0.90**	0.00	0.03	0.30	**0.80**	0.21	0.00	0.20	**0.96**	0.00
$MS4_{num}$	0.02	0.00	0.00	**0.65**	0.00	0.08	0.27	**0.89**	0.00	0.07	0.16	**0.92**
Mode shape	$MS1_{exp}$	$MS2_{exp}$	$MS3_{exp}$	$MS4_{exp}$	$MS1_{exp}$	$MS2_{exp}$	$MS3_{exp}$	$MS4_{exp}$	$MS1_{exp}$	$MS2_{exp}$	$MS3_{exp}$	$MS4_{exp}$

The time required for each analysis of each adjusted model was the last parameter investigated in the work. Model A required the least amount of time, while Models B and C were 1.4 and 4.1 times slower, respectively. This difference in analysis time of the first two models when compared to the last was expected due to the additional degrees of freedom in the third model, which had 546,399 DOF when compared to the 13,320 DOF of Model A and 20,556 of Model B. This data is relevant in the context of this work, as the time to generate the necessary database for the next stage of the evaluation procedure can be a crucial factor in the selection. For the case study, Model C will take four times longer than the others to build the database. However, the choice of this model in the present study is justified by the greater accuracy achieved in the relevant calibration parameters previously discussed, especially the MAC values. Thus, model C was for constructing the database and computing damage indices. One limitation of the model is its simplified approach for representing damage, which relies on penalizing flexural stiffness (EI) instead of explicitly modeling crack propagation using advanced techniques like XFEM or VCCT. While these methods could offer more detailed fracture mechanics insights, they would significantly increase computational time. The chosen approach ensures that modal displacements are effectively captured while maintaining computational efficiency. This simplification was crucial for generating a large database of damage scenarios required for training neural networks, enabling a balance between accuracy and feasibility in large-scale structural health monitoring applications.

7.2.
Model calibration

After selecting model C for further adjustment, five additional calibration steps were added for a finer tuning of its dynamic response. The errors (ε) measured at natural frequencies during each model update phase are shown in Fig. 27 for the four initial mode shapes (MS1 to MS4), according to Table 5 appearance order. From the first to the third stages, the springs stiffness at the end

supports were adjusted. The soil spring coefficient was estimated by multiplying the values provided by Terzaghi for stiff clays in the plate load test by the area of the viaduct's wing walls, ranging from $4.49E+06\ N/m$ to $3.80E+07\ N/m$. In the fourth and fifth stages, the Young's modulus, based on the field measured f_{ck}, were assigned to the girders. In the sixth step, the New Jersey barriers mass was added to the deck. In the seventh stage, the approach slab mass was incorporated into the viaduct model edges. The mass added by the slab was calculated considering it as reinforced concrete, with a density of 2500 kg/m³. With an area of 31.2 m² and thickness of 0.25 m, the resulting mass was 19500 kg. The eighth update step consisted of adjusting the spring stiffness of the intermediate columns supports based on the field test results. The last two stages involved adding the asphalt layer mass to the model. The mass added to the model due to the asphalt, with a density of 2400 kg/m³, varied according to the thickness adopted in the calculations. Initially, a thickness of 0.15 m was considered over an area of 417.3 m², resulting in a mass of 150228 kg. Subsequently, the thickness was adjusted to 0.25 m, which increased the mass to 250380 kg in the model. The asphalt layer thickness was increased to obtain a modal response closer to the experimental, since it was not possible to remove an asphalt sample in situ for the evaluation of this parameter. The initial and final values for the previously mentioned parameters can be found in Table 12. It can be observed that the steps that showed the parameters with major impact in reducing the relative error between natural frequencies were those that altered the model's boundary conditions.

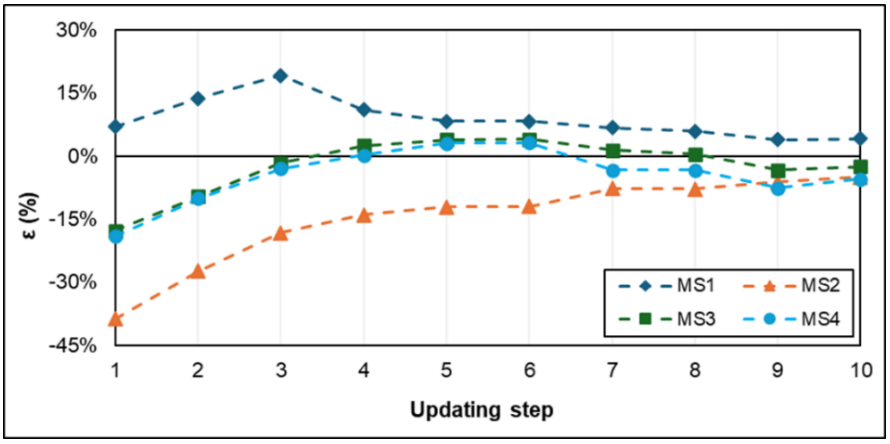

Figure 27 - Model updating steps results

Table 12 - Initial and final valued for the adjusted parameters

Parameter	Initial value	Final value
Wings springs stiffness (N/m)	4.49E+06	3.60E+07
Left girder elasticity modulus (GPa)	31	34
Right girder elasticity modulus (GPa)	31	35.5
New Jersey barrier mass (kg)	0	16050
Approach slab mass (kg)	0	19500
Columns spring stiffness (N/m)	5.00E+07	7.20E+08
Asphalt layer mass (kg)	150228	250380

Table 13 shows a comparison between the natural frequency values before and after model calibration. The measured difference (Δ) highlights the effectiveness of the update by approaching the numerical and experimental responses. The last three natural frequencies of the numerical model were more susceptible to adjustments than the last one. The difference between the natural frequencies obtained experimentally and numerically was less than 1Hz, that is, with an error (ε) equal to or less than 5%.

Table 13 - Numerical and experimental natural frequencies comparison

Mode shape	Numerical model		$\lvert \Delta \rvert$	Experimental	ε (%)
	Initial (Hz)	Natural Freq. (Hz)		Natural Freq. (Hz)	
1	5.20	**5.33**	3%	5.59	5%
2	14.55	**11.07**	24%	10.49	-5%
3	15.96	**13.89**	13%	13.55	-2%
4	21.57	**19.11**	11%	18.13	-5%

Figure 28 shows the modal participation factors. The first fifteen natural frequencies obtained by the calibrated model are shown on the horizontal axis. At the same time, each modal participation in the y-component is presented on the vertical axis. The higher values observed ensure these four mode shapes choice for the update stage, as they ensure their significant contribution to the overall behavior of the system under vibration. The numerical modes and their respective frequencies can be seen in Figure 29.

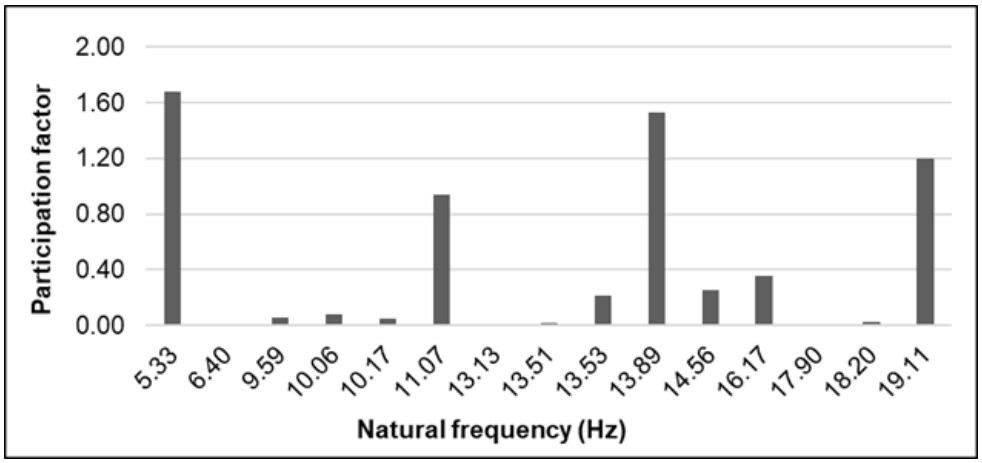

Figure 28 - Participation factor in vertical component

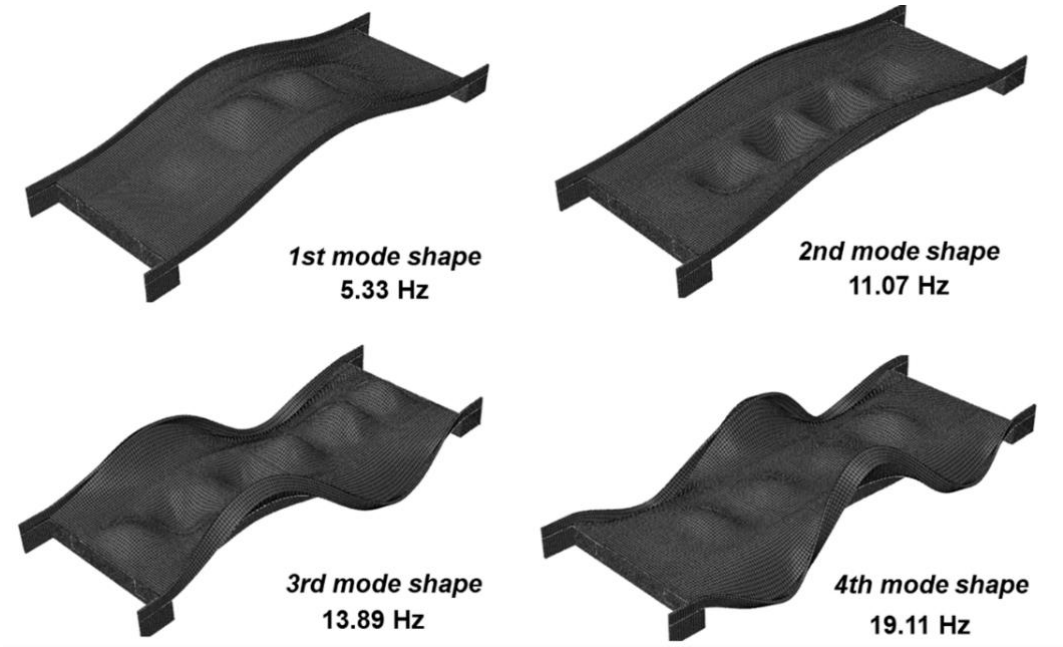

Figure 29 - Viaduct mode shapes

Figure 30 shows the values obtained for MAC. The indices for the four identified vibration modes were equal to or greater than 0.85, indicating a reasonable correspondence between the mode shapes. A significant similarity between the first and second vibration modes is observed, as indicated by the close values off the main diagonal. This same behavior was noticed experimentally, with the difference being the separation between the natural frequency values of the two modes.

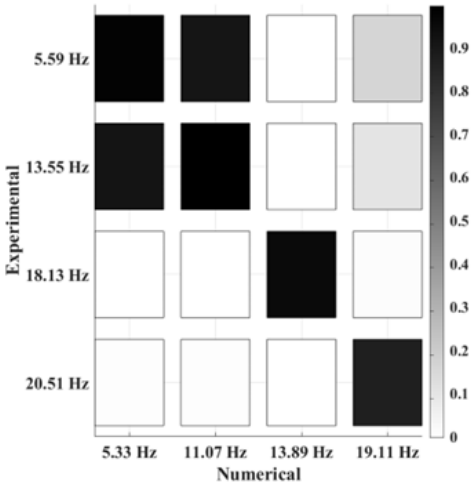

Figure 30 - MAC results

Table 14 presents the MAC and MMI indices. The comparison of results before and after the model update highlights the improved alignment between the experimental and numerical frequencies achieved through calibration. The largest differences were observed in the first three modes, with less significance for the highest of them. The values obtained for MAC confirm the similarity between the vibration mode shapes, with values closer to 1 for the first three modes. Based on these findings, it can be concluded that the calibration process becomes more complex as the natural frequency increases.

Table 14 - MAC and MMI results

Mode shape	MAC		MMI	
	Initial	Final	Initial	Final
1	0.98	0.99	0.43	0.47
2	0.99	1.00	0.40	0.48
3	0.95	0.96	0.31	0.49
4	0.85	0.87	0.19	0.41

The Modal Matching Index (MMI) was used to thoroughly assess the performance of the modal properties. Its maximum value is equal to the initially assigned weight (0.5), indicating a perfect match in both natural frequency and modal shape. The values in Table 8 are within a reasonable range, demonstrating a closer correspondence for all mode shapes. The impact of model updating on these results can be better understood by referencing the data in Figure 31. It is evident that in all cases, the natural frequencies and modal shapes tended to converge.

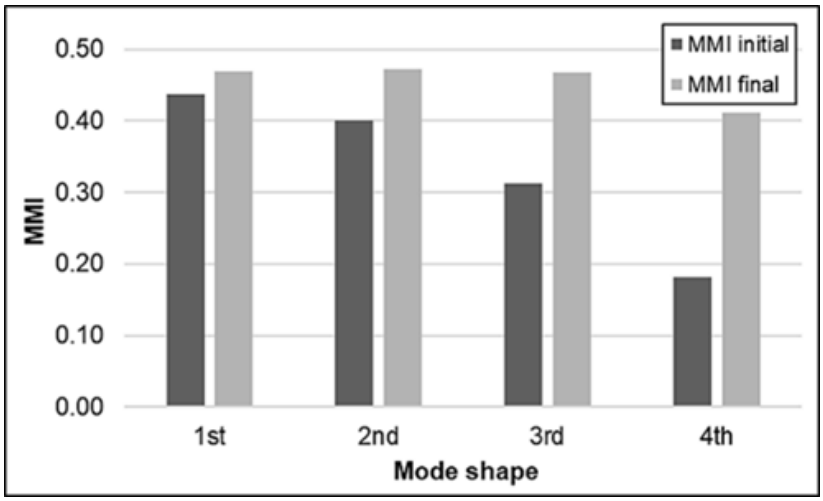

Figure 31 - MMI values for initial and updated states

The results presented in Tables 14 and 15 were compared with finite element model updating methods employed by other authors. In the present work, the manual updating focused on three aspects: adjusting the spring stiffness at the supports, defining the mass of elements such as the deck, and modifying the stiffness by adjusting Young's moduli of materials. This strategy reduced the average frequency error to 4.5% and resulted in a Modal Assurance Criterion (MAC) of 0.89 or higher for the vibration modes. In comparison, Teughels [107] adjusted the Young's and shear moduli, obtaining frequency differences of less than 1% and MAC greater than 0.8. Altunisik and Bayraktar [43] focused on material properties and constraints, reducing errors from 49.1% to 0.6% and achieving high modal correlation. De Angelis and Pecce [44] combined static and dynamic tests to adjust vertical stiffness and modulus of elasticity, resulting in differences of less than 5% between numerical and experimental natural frequencies and a MAC ranging between 0.96 and 0.98. Thus, the close alignment between experimental and numerical results, consistent with other studies, underscores the effectiveness of the methodology in accurately representing the structural behavior of the viaduct.

7.3.
Partial conclusions

An important part of this process was the selection of the modeling strategy. The main conclusions that could be drawn from this phase were:

- The unique disadvantage of model C when compared to the others was its larger processing time. Each analysis took more than three times the

average time taken by the other two models. Therefore, creating the database was a time-consuming task.

- When comparing natural frequencies, Model C showed a better fit to the experimental data when compared to Models A and B. To further justify the selection of Model C, the MAC parameter was also considered. The MAC values, approximately 8% higher in Model C, indicated greater agreement between the numerical and experimental mode shapes, making it the most suitable model for database creation.
- The choice of Model C can also be justified by its ability to more accurately represent the behavior of structural elements subjected to damage. By simulating the introduction of damage through the reduction of flexural stiffness in the lower portion of the longitudinal beams, Model C can capture more realistically the crack concentration in that region.
- Beyond the aspects already discussed, it is necessary to discuss the results of models A and B. In the case of model A, a significant discrepancy was observed between the numerical and experimental natural frequency values, especially in the first vibration modes. This difference may be related, in part, to the type of element adopted, two nodes instead of three nodes beam, in the discretization of the model and the absence of auxiliary elements capable of adequately representing the additional bending stiffness provided by components such as guardrails and New Jersey barriers. Model B showed superior performance compared to model A, with smaller absolute errors in natural frequencies and better MAC values, especially in the first three modes, although not with the same degree of precision achieved by model C.
- The increase in the spring coefficient of the wings and abutments resulted in a significant reduction in the percentage of measured error (ε). During stages 1 to 3 of the update, an average reduction of 10% in the size of the error in the natural frequencies was observed, with a greater impact on the last three vibration modes.
- After the boundary conditions were adjusted, the most significant steps in numerical model updating were the increase in the material's modulus of elasticity (E) and the mass addition to the deck, respectively. Adjusting the modulus of elasticity proved effective in reducing the error associated with the first vibration mode, with a 5% reduction observed in steps 4 and 5 of the update process. The final mass of the model, which is one of the

uncertainty sources in the data, played a key role in structure dynamic behavior fine-tuning. Steps 6 to 10, dedicated to this adjustment, resulted in a 4% reduction in the average error of natural frequencies.

8.
Damage diagnosis

8.1.
Damage indicator

Two damage indices were considered for damage detection. The results obtained using the first of the two indices, the modal curvature, for two different damage positions are presented in Figures 32 and 33 for damage location at 10 m and 20 m, respectively. The vertical axis represents the difference between the values of the intact and damaged modal curvatures (Δk), while the horizontal axis extends along the entire length of the longitudinal beam. There is a clear difference between the results at the damaged point and the others, especially for more severe damages, indicating the presence and the defect place. The gap between the vertical axis Δk values at the same damaged point highlights the difference between the distinct damage severities. Similar behavior can be observed at different points along the beam, both at 10m (Figure 32) and at 20m (Figure 33).

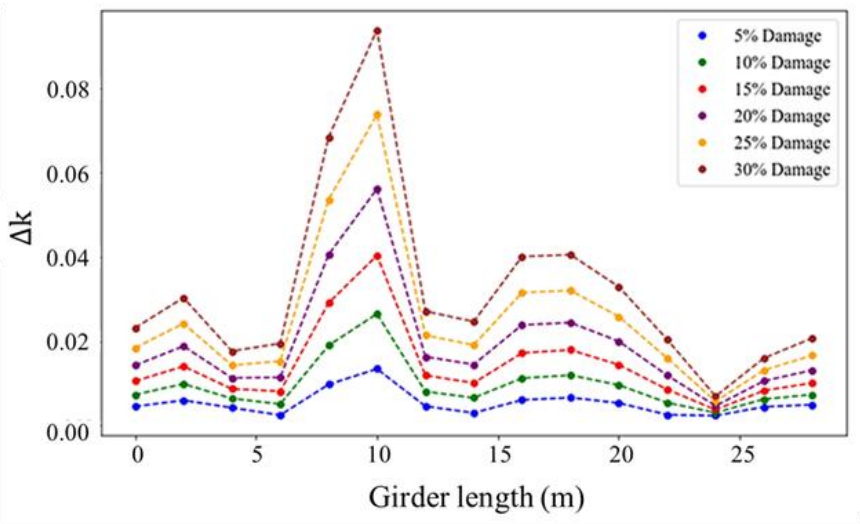

Figure 32 - MCM result for damage at 10m

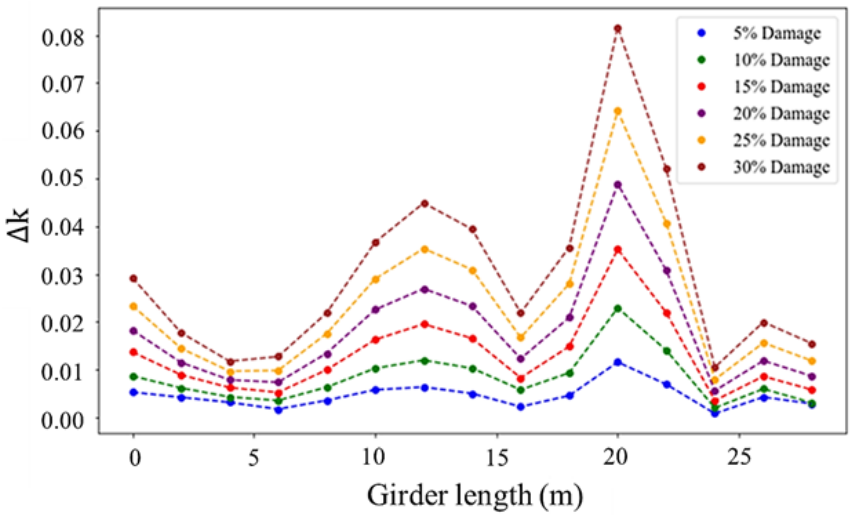

Figure 33 - MCM result for damage at 20m

Figures 34 and 35 show the results obtained when the modal strain energy index is used. The ordinate axis shows the standardized value of the indicator (Z), while the abscissa axis extends along the length of the longitudinal beam. The behavior observed in this indicator presents two prominent peaks, the largest of which is at the location where the artificial damage was introduced. There is a slight difference between the damage intensities when compared to the modal curvature index. As in the previous case, the result was similar in different sections of the structure.

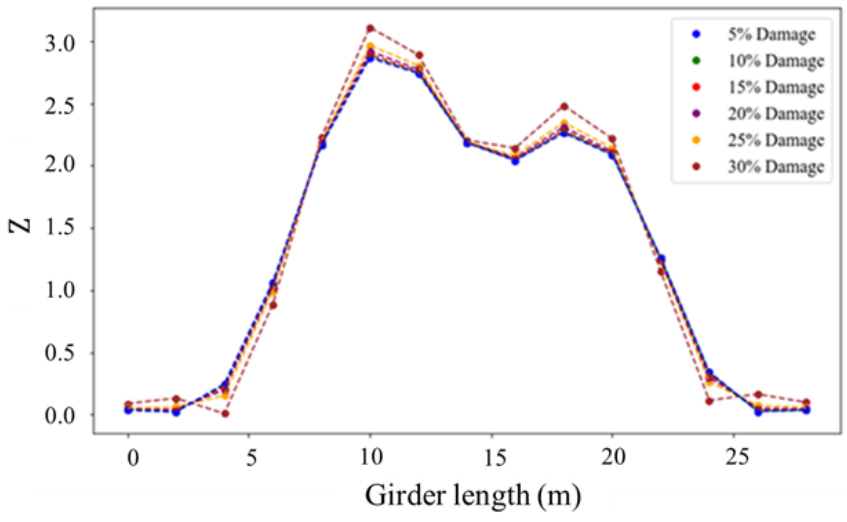

Figure 34 - MSE result for damage at 10m

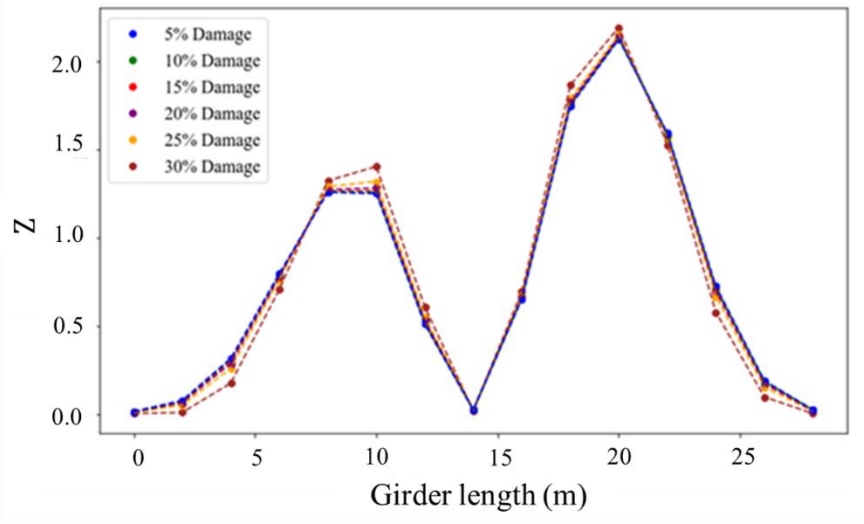

Figure 35 - MSE result for damage at 20m

The modal curvature showed more reliable results when compared to the modal strain energy. The unique and prominent peak at the damaged point indicates the interest zone, in contrast to the strain energy results. Therefore, the study proceeded using only the modal curvature results as ANN input.

8.2. ANNs architecture and performance

The choice of neural network architecture significantly affects prediction accuracy. As discussed in section 2.4, the number of neurons per layer and activation functions change depending on the problem and are almost unique, meaning they cannot simply be replicated from one case to another. Consequently, the study conducted tests to identify the best architecture for the two neural networks proposed for the system.

The first artificial neural network architecture was developed to identify and locate structural damage. This represents a multilabel classification problem, in which each output belongs to a distinct category. Two parameters were evaluated during development: number of neurons and hidden layers and the activation functions. The input and output layers remained the same across all configurations. The input layer contained 30 neurons, each receiving a modal curvature value. The output layer consisted of 7 neurons corresponding to the possible classifications (6 for the different damage positions and 1 for the undamaged state). Table 15 presents the architecture tested for the classification problem. In the MCL1 and MCL2 models, the network features two hidden layers: the first contains a number of neurons equal to the average of those in the input and output layers, while the

second contains half that value. This configuration aims to balance the ability to extract patterns without excessively increasing complexity. For more complex problems, the MCL3 and MCL4 models employ the controlled expansion rule, which increases the number of neurons in the first hidden layer and then progressively reduces them in the subsequent layers. Finally, the MCL5 and MCL6 models adopt a structure in which there is a gradual reduction in neurons starting from the first hidden layer, which is composed of half the neurons in the input layer. The *tanh* function maps inputs to a range between -1 and 1, centering the data and often improving convergence during training. ReLU, on the other hand, is computationally efficient and helps mitigate the vanishing gradient problem by allowing gradients to flow more effectively during backpropagation. Additionally, ReLU's tendency to output zero for negative inputs often produces sparse representations that aid in regularization and reduce overfitting. In this work´s models, *tanh* was applied to even-numbered models, while ReLU was used in the hidden layers of odd-numbered models.

Table 15 - Damage location ANNs tests results

ANN	Hidden layers		Evaluation		
	Neurons	Activation function	Precision	Recall	F1-Score
MLC1	18 | 9	ReLU	0.79	0.80	0.79
MLC2	18 | 9	Tanh	0.84	0.86	0.85
MLC3	64 | 32 | 16	ReLU	0.46	0.57	0.51
MLC4	64 | 32 | 16	Tanh	0.71	0.70	0.70
MLC5	15 | 12 | 9	ReLU	0.81	0.87	0.83
MLC6	15 | 12 | 9	Tanh	0.91	0.93	0.92

More details about the results of the MLC6 neural network are shown in Figure 36. The confusion matrix vertical axis refers to the true results, while the horizontal axis is for the predicted results. Cells on the main diagonal represent true positives, where the model predictions match the true labels. Therefore, intersection values outside the main diagonal indicate incorrect predictions made by the model. Values labelled as zero refer to undamaged scenarios, while the others represent the sections in the longitudinal girders divided into six parts. The ANN results for validation and training stages with modal curvature index input are shown in Figures 36a and 36b, respectively. A small deficiency may be noted when predicting damage in the first and third sections of the longitudinal beam, indicated by the false negative values. However, the accuracy rate remained within an acceptable margin, equal to 91% on average across all classes.

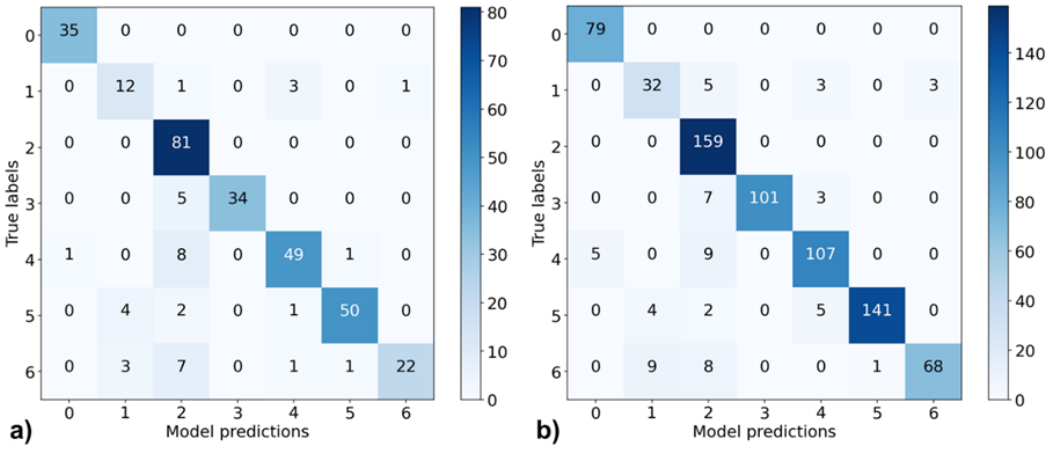

Figure 36 - Damage detection network a) Validation b) Training

Table 16 summarizes the selected metrics for each class of the classification problem based on the validation data. The high precision and recall values suggest that the ANNs are performing satisfactorily. The high overall performance in the validation set, which was not present in the training phase, suggests that the ANN is effective in generalizing its predictions.

Table 16 - Damage detection ANN metrics results

Target	Precision	Recall	F1-score
Undamaged	0.94	1.00	0.97
1st section	0.71	0.74	0.73
2nd section	0.84	1.00	0.91
3rd section	1.00	0.91	0.95
4th section	0.91	0.88	0.90
5th section	0.99	0.93	0.96
6th section	0.96	0.79	0.87
Weighted average	**0.91**	**0.93**	**0.92**

The architecture testing procedure, initially applied for damage identification, was replicated for the neural network tasked with estimating damage severity—a subsequent phase in the system's diagnostic workflow. During this stage, the performance metrics defined in section 2.2—Mean Absolute Error (MAE), Mean Squared Error (MSE), Root Mean Squared Error (RMSE), and the coefficient of determination (R^2)—were evaluated. All tested models shared identical input and output layer configurations: the input layer comprised 30 neurons, each corresponding to a modal curvature value from the dataset, while the output layer contained a single neuron utilizing a linear activation function to generate severity

estimates. Table 18 summarizes the architectures explored in this phase, detailing their layer configurations and activation functions.

Table 17 - Severity estimation ANNs tests results

ANN	Hidden layers		Evaluation			
	Neurons	Activation function	MAE	MSE	RMSE	R^2
R1	18 | 10	ReLU	0.027	0.001	0.038	0.858
R2	18 | 10	Tanh	0.034	0.003	0.052	0.801
R3	64 | 32 | 16	ReLU	0.087	0.010	0.101	0.710
R4	64 | 32 | 16	Tanh	0.044	0.003	0.052	0.703
R5	25 | 15 | 5	ReLU	0.010	0.001	0.026	0.920
R6	25 | 15 | 5	Tanh	0.037	0.024	0.153	0.767

The analysis of the architectures in table 18 provides insight into the relationship between model complexity, activation functions, and performance metrics. The best-performing model (R5) achieved superior results (MAE: 0.010, MSE: 0.001, RMSE: 0.026, R^2: 0.920) with a balanced three-hidden-layer architecture, demonstrating that moderate depth combined with the non-linearity of the ReLU function can achieve reasonably accurate predictions for the problem. In contrast, simpler architectures, such as R1 and R2, showed that ReLU outperforms Tanh (R1: R^2=0.858 versus R2: R^2=0.801), highlighting ReLU's advantage. Deeper networks, such as R3 and R4, exhibited reduced performance (R3: R^2=0.710; R4: R^2=0.703), suggesting that additional layers can lead to optimization challenges. Overall, ReLU activation consistently delivered more robust results across all configurations, while model depth requires careful calibration: too few layers limit expressiveness, and too many introduce instability. The optimal balance, observed in R5, combines strategic reduction of layers with ReLU's robustness to achieve minimal error and maximum explanatory power ($R^2 \approx 0.92$).

Given the 0.05 discretization steps, the network’s predictions demonstrate excellent accuracy. The MAE of 0.0095 indicates that the average absolute difference between predicted and actual damage values is minimal. Additionally, the MSE of 0.0007, which penalizes larger errors more severely, reinforces the model's overall accuracy. The RMSE of 0.0264, while slightly higher than the MAE, remains within an acceptable range, suggesting that the model’s predictions are typically within a small margin of error from the true values.

Figure 37 shows how the regression Artificial Neural Network (ANN) predicted values compared to real values. The R^2 value of 0.92 is strong, meaning the model accounted for 92% of the variation in the data. Most points on the scatter

plot are close to the perfect fit line, indicating accurate predictions. However, there is some spread, especially for higher values.

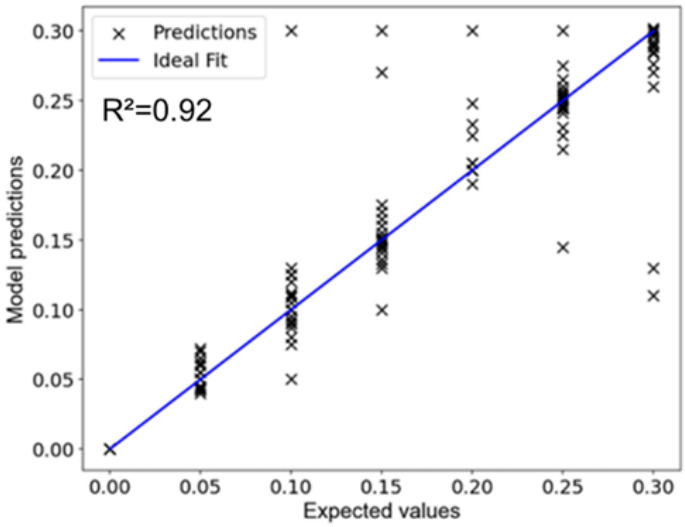

Figure 37 - Damage severity networks performance

The final architecture of systems ANNs is summarized in Table 18.

Table 18 - ANN's final architecture

ANN	Input layer	Hidden layers			Output layer		Training parameters		
	Neurons	Layers	Neurons per layer	Activation function	Neurons	Activation function	Learning rate	Epochs	Loss function
Damage detection	30	3	15 | 12 | 9	Tanh	7	Sigmoid	0.01	500	Categorical cross entropy
Severity estimation	30	3	25 | 15 | 5	ReLU	1	Linear	0.002	550	Mean squared error

8.3.
Partial conclusions

The modal curvature (MCM) emerged as a more reliable indicator than modal strain energy (MSE) for identifying damaged areas. Its distinctive peak effectively highlighted the damaged region, supporting its choice for the neural network input. About the damage indicator choice, it can be concluded that:

- The Modal Strain Energy (MSE) indicator did not consistently yield clear localization, thereby supporting the decision to rely primarily on MCM for damage detection.
- The reliability of MCM in isolating damage signatures directly contributes to the high accuracy of both the damage detection and severity estimation networks.

The ANNs proved effective in diagnosing the structural condition. Besides this main conclusion, the following was also observed:

- A moderate-depth network (e.g., the three-hidden-layer configuration of model R5) provided an optimal balance between expressiveness and training stability, achieving high accuracy ($R^2 \approx 0.92$, $MAE \approx 0.010$) with minimal error, while deeper architectures tended to introduce instability.
- The gradual reduction in neuron count across hidden layers helps to efficiently extract relevant features from the modal curvature input enhances overall network performance.
- The neural networks, utilizing modal curvature data as input, achieved a damage localization accuracy of over 90%.
- The neural network using the Modal Curvature method as input proved to be accurate in diagnosing the severity of the damage. The distinct characteristics of the peaks caused by the imposed damage, as evident in the results, enable the neural network to effectively distinguish them. The same cannot be said about the Modal Strain Energy method, which did not produce reliable results.
- The generalization capability of the model was demonstrated by the validation results. The R^2 value above 0.92 indicate that it was able to make accurate predictions with data outside the training group.

9.
BIM and SHM integration

9.1.
Tools

The integration presented in section 5.5 was carried out through the *PyRevit* extension in a BIM model developed in Autodesk Revit. *PyRevit* enables the execution of Python extensions within the BIM environment, provided they follow a previously defined folder structure. As illustrated in Figure 38, this structure requires that the main folder, called *.extension*, contains all the extension content, organized into two subfolders: *.lib*, which includes the Python libraries used by the scripts — such as *TensorFlow* and *Scikit-Learn* for machine learning, and *Numpy* and *Pandas* for matrix operations and dataframe manipulation — and *.tab*, which contains all the extension tab components, organized in *.panel* type subfolders. Additionally, each extension function must be in a.*pushbutton* folder, which includes the Python *script* and the icon displayed in the graphical interface. The integration carried out in this work resulted in the SHM tab creation (Figure 39), divided into three panels: *Asset Overview, Bridge Inventory*, and *Structural Diagnosis*.

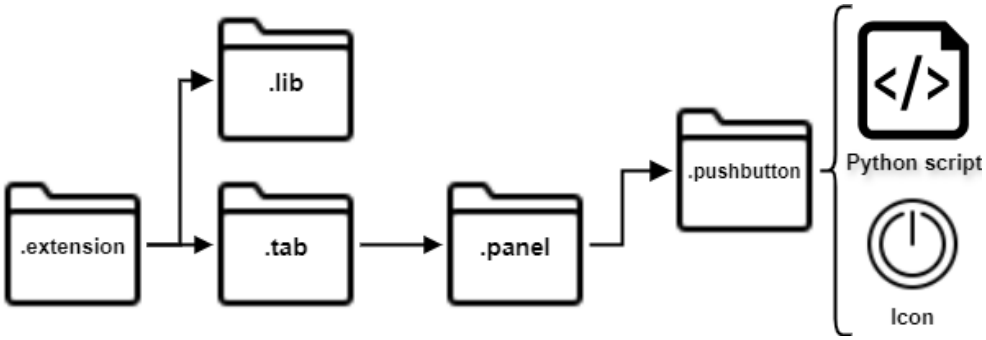

Figure 38 - PyRevit fold structure

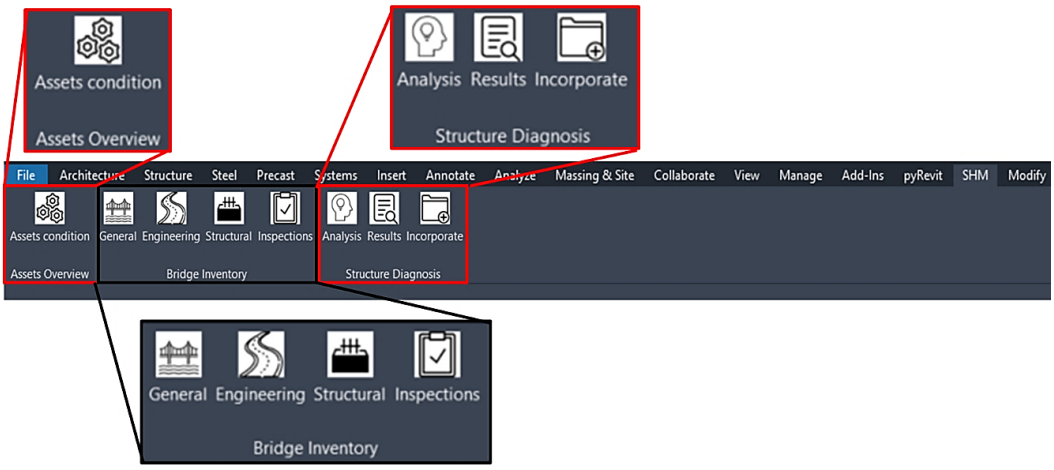

Figure 39 - SHM tab overview

The *Assets Overview* panel directs the user to an online dashboard with information about other managed assets (Figure 40). This dashboard provides a clear, visual summary of bridges and viaducts conditions, highlighting key issues such as joint deterioration and other concrete pathologies. By linking directly to a BIM platform via a PyRevit *.urlbutton*, the engineering team can seamlessly switch between the model and the dashboard, ensuring real-time updates and a single source of information. This integration enables collaboration among stakeholders, quicker identification of critical issues, and efficient resource allocation, ultimately improving the long-term management and maintenance of infrastructure assets.

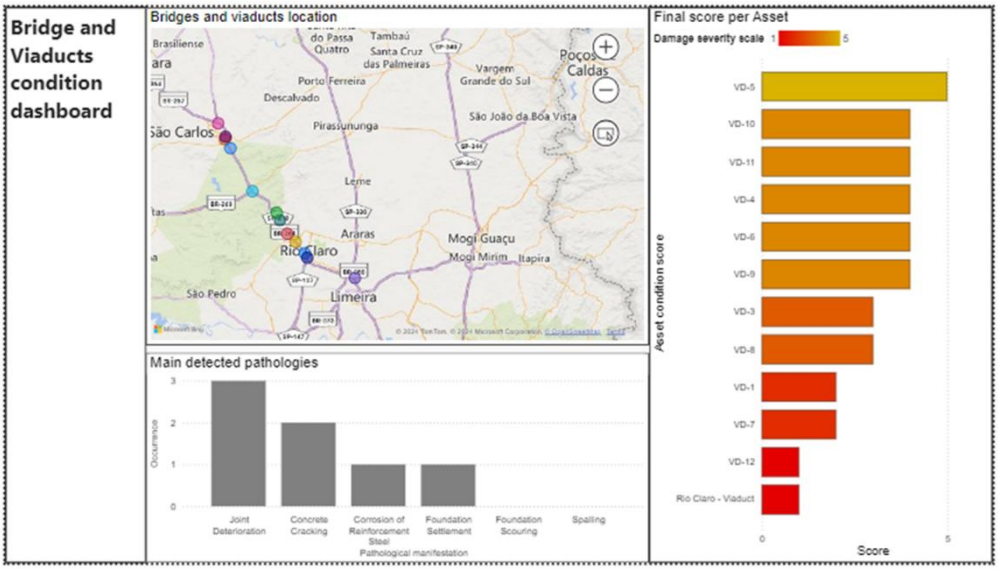

Figure 40 - Assets Overview dashboard

Access to the viaduct inventory, available in the second panel of the SHM tab, is organized into specific buttons for *general*, *engineering*, *structural*, and *inspection history*. The first three options display the information in a single window

(Figure 41a), while the *inspection history* button opens an initial screen for selecting the desired report before viewing the content (Figure 41b). This part of the integration enabled the use of the BIM model as a digital and centralized information repository. With all data concentrated in a single environment, decision-making becomes more agile and precise.

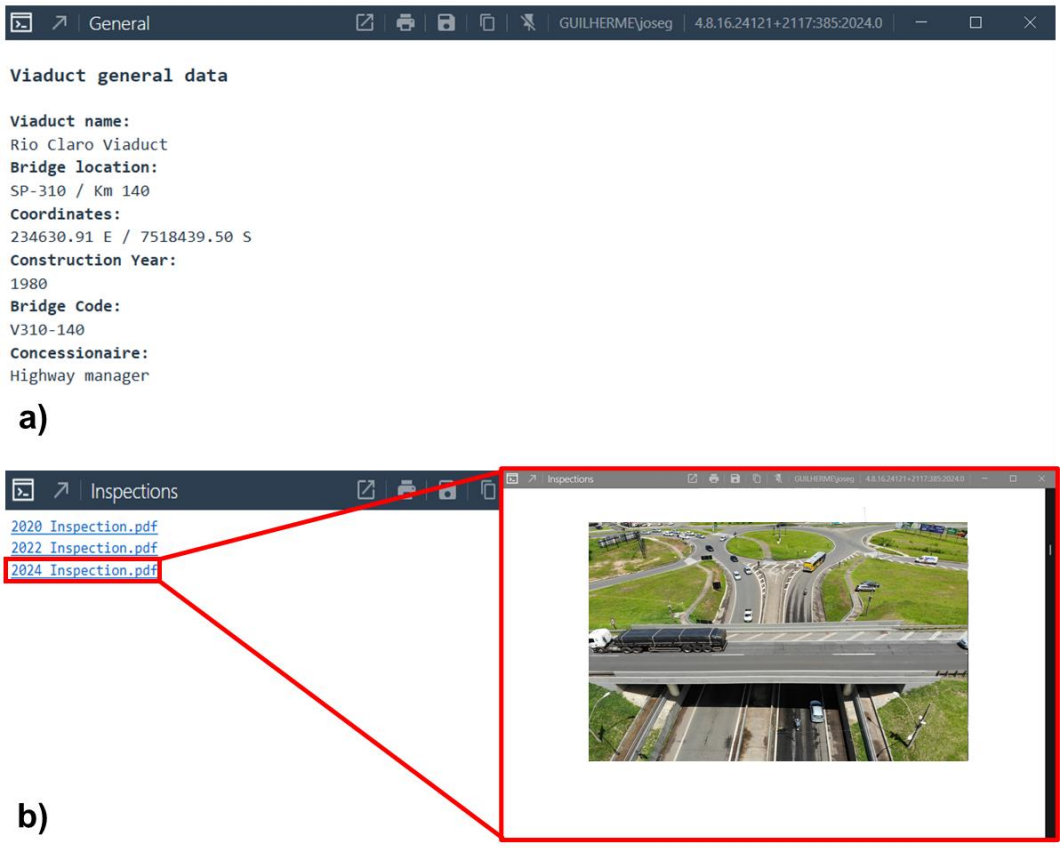

Figure 41 - Viaduct's a) General data window and b) Inspection history windows

The third panel is dedicated to structural diagnosis. The *analysis* button applies two pre-trained neural networks to identify damage and evaluate its severity. The results of this analysis are compiled into a report, which is stored in the a data repository. To perform the analysis, an input file containing modal curvature data, experimentally collected from 30 points on the viaduct, must be available in the CDE. The *incorporate* button allows the report's findings to be integrated into the BIM model, updating the design properties of both intact and damaged longitudinal beams. This process ensures the digital twin remains up-to-date and enhances the information model (Figure 42). Additionally, the *report* tool aggregates data from all girders, generating a color-coded visualization of the model. This visualization, accessible online, provides the manager with a clear and comprehensive overview of the structure's current condition.

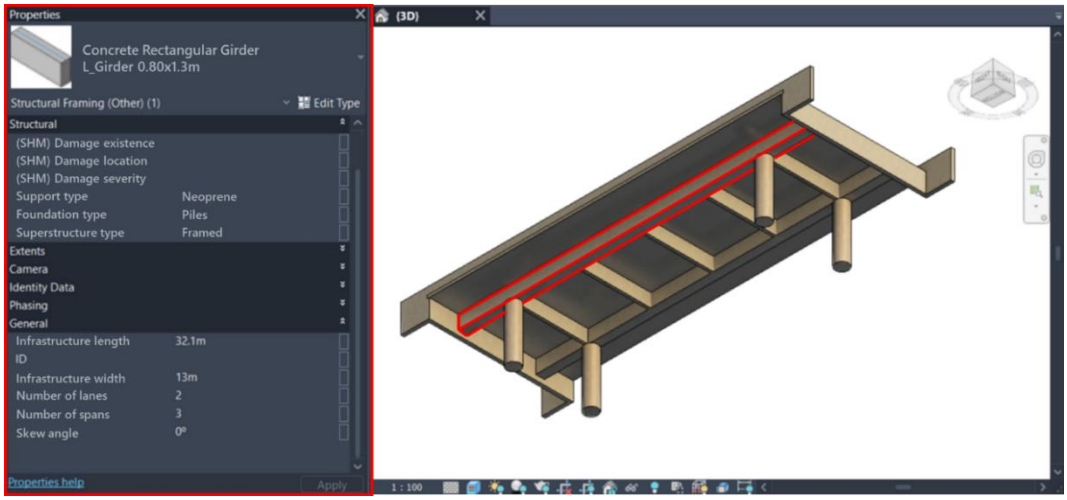

Figure 42 - *Incorporate* button result

9.2.
System tests

Two tests were conducted using the developed system developed for the Rio Claro Viaduct. The first aimed to evaluate the neural network's ability to make predictions for data not used during their training. To this end, a new dataset was generated from the same numerical model but with different damage levels and distributions than those considered previously. The second test aimed to verify the full end-to-end functionality of the system. In this test, data from a second field experiment, conducted ten years after the first, were used. Note that the data was collected at the same thirty points on the viaduct.

Figure 43 shows the neural network's results applied to the new dataset. Compared to the validation results, a slight drop in performance (5%) is observed for the adopted metrics (precision, recall, and F1-score) in the detection and localization ANN (Figure 43a). This variation is understandable, given the greater dataset diversity. Even so, the accuracy rate remains above 85%. The neural network responsible for assessing damage severity also maintains the previous performance, with a coefficient of determination (R^2) of 0.96 (Figure 43b). The mean absolute error of 0.005 is significantly smaller than the smallest difference in damage intensity present in the test data (0.02), indicating high prediction accuracy. These results demonstrate that the networks are able to generalize and do not suffer from overfitting.

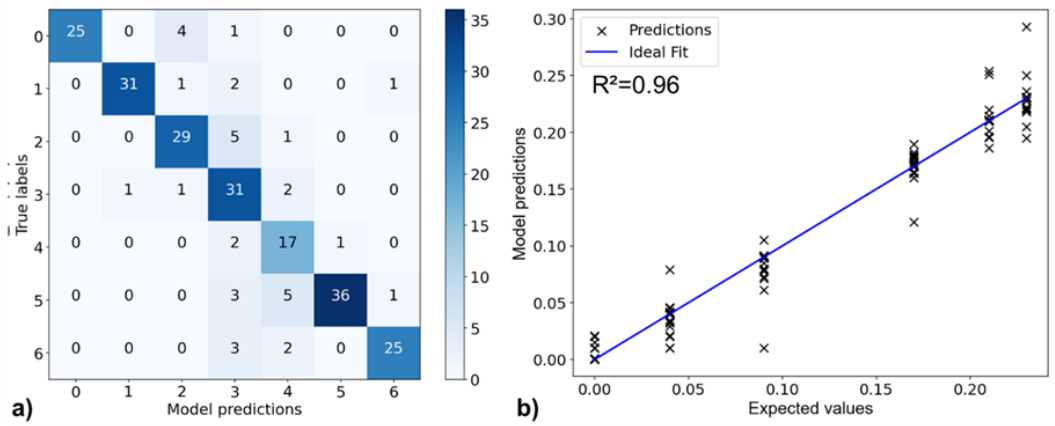

Figure 43 - a) Classification performance b) Regression performance

The modal curvature used in the final benchmark was derived from the mode shapes obtained during the ambient vibration test conducted in 2024. These results were used as input to the proposed system, which is integrated to the BrIM model, the output indicated no damage presence in the Rio Claro Viaduct longitudinal girders. The report generated from this result is shown in Figure 44 showing that the asset has preserved its structural integrity after the 10-year period.

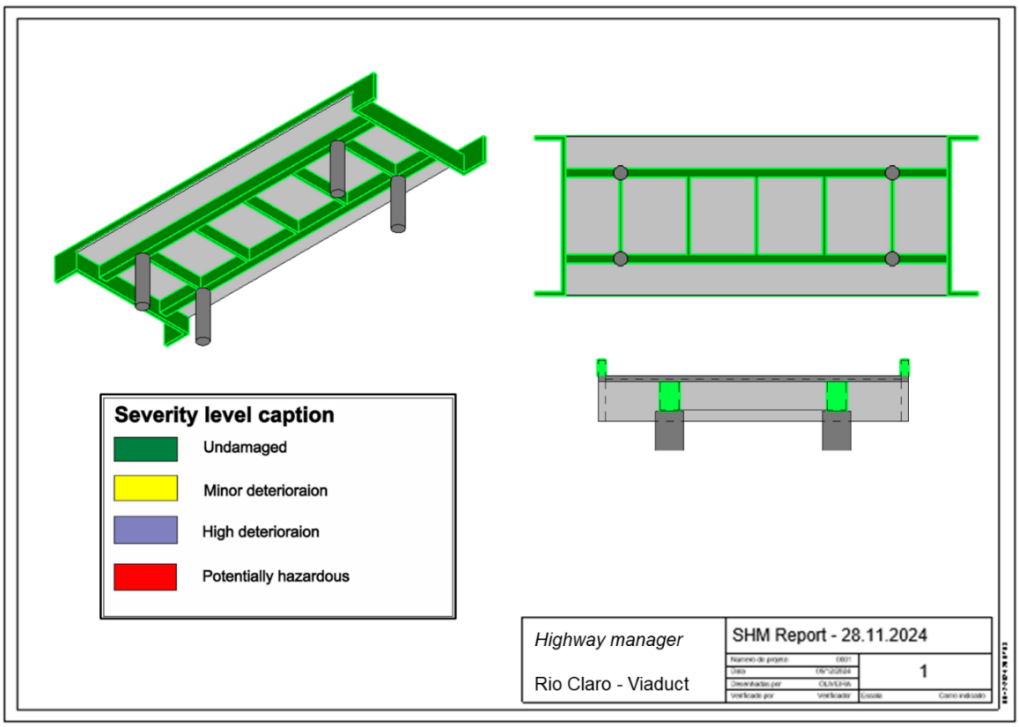

Figure 44 - Structure condition report

It can be noted that the natural frequencies remained relatively constant over the ten years, varying by an average of 1%, indicating that the analyzed structure

did not experience significant changes in its stiffness. This confirms results obtained from the developed system's result.

9.3.
Partial conclusions

The case study of the Rio Claro Viaduct demonstrates the framework's potential. Field tests provided accurate dynamic characteristics, which were used to fine-tune the finite element model. Simulated damage scenarios enabled the training of ANNs that effectively correlated modal curvature indices with the extent and location of structural degradation. The detection and localization network maintained high performance, achieving over 85% accuracy even when tested on a dataset with varied damage levels, while the damage severity network yielded an R^2 of 0.96 with minimal mean absolute error. This corroborates the neural networks' assessment of the structure's has preserved its condition over the 10-year span. These results collectively validate not only the individual components' accuracy but also the overall system's capability to provide reliable structural health assessments over extended periods of time.

The proposed framework combines field data, numerical models, and predictive analytics in a Building Information Modeling environment using *PyRevit*. This unified three key structural health monitoring components: characterization of structural behavior, model-based diagnostics, and data-driven prognostics using artificial neural networks. By centralizing this information, the DT enables intuitive visualization, accurate structure's condition updates and reliable decision-making. The case study demonstrated the framework's replicability by using BIM's inventory and dynamic inspection data to address problems in existing SHM systems, such as fragmented historical records. The system automatically locates and quantifies damage, connecting theoretical models with practical insights by directly updating BIM elements with damage information. This integration improves data visualization and reporting, which can lead to effective maintenance planning decisions.

10.
Conclusion

The experimental tests carried out on the Rio Claro viaduct in 2014 and 2024 demonstrated the effectiveness of the proposed approach for characterizing modal properties. The dense experimental mesh, with 30 points distributed along 32.1 m, ensured detailed capture of the mode shapes, minimizing undersampling effects and noise. The redundancy in modal identification, through EFDD (frequency domain) and SSI-COV (time domain) techniques, validated the reliability of the results, with MAC correlation ≥ 0.8 between modes and frequency discrepancies $\leq 1\%$. The stability of natural frequencies over 10 years (variation ≤4.5%) and the maintenance of damping factors (3–5%) confirmed the structural integrity, aligning with the objectives of evaluating temporal changes and validating the contribution of the experimental program for model calibration and obtaining damage indicators.

The numerical approach stood out for the selection of Model C (solid elements), which, despite the higher computational cost, showed superiority in correlation with experimental data (MAC ≥ 0.90 and error $\leq 5\%$ in frequencies). The manual calibration, focused on adjustments of stiffness (modulus of elasticity) and mass (asphalt thickness and additional elements), refined the representation of dynamic behavior. The generation of 1,120 artificial damage scenarios, simulated via reduction of flexural stiffness (EI), allowed the creation of a robust database for training neural networks, fulfilling the objective of exploring modeling strategies and parameter sensitivity. The precision achieved reinforced the viability of using updated models to simulate physically unfeasible scenarios, essential for structural diagnostics.

The damage detection methodology employed the Modal Curvature Method (MCM) as input for artificial neural networks (ANNs), outperforming the Modal Strain Energy Method (MSE) in reliability. The system was structured in two sequential stages: the first, which identifies the presence and location of damage in predefined sections, and the second, which estimates the severity of the damage. The ANNs achieved accuracy greater than 90% in damage location and R^2=0.96 in severity estimation, with a mean absolute error of 0.0095, validating their effectiveness even with data not seen in the training phase. This performance met the objective of developing a tool for structural diagnosis, mitigating external

interference, and reducing human uncertainties. The generalization of the networks, proven in the tests of section 9.2, highlighted their potential for application in various monitoring scenarios.

The integration between the SHM system and BIM methodology was successfully carried out through the *PyRevit* extension in *Autodesk Revit*, consolidating multidisciplinary data (inspection history, dynamic properties, and diagnostics) in a common data environment. The automation of integrity reports and interactive visualization in the digital twin allow for data-driven decision-making and align to create a single platform for asset management. The dynamic updating of the BIM model with ANN results demonstrated the feasibility of transforming technical data into actionable insights, potentially assisting in decisions about interventions in the structure and extending the asset's useful life.

Future research could expand on this thesis by addressing complementary topics. First, automating critical phases, such as model calibration and damage report creation, of the workflow could enhance efficiency, reduce human intervention, and minimize errors in the structural health monitoring process. While the current damage detection algorithm focuses on identifying stiffness loss in the viaduct’s longitudinal girders, it does not account for other potential failure modes, such as abutment settlement, expansion joint degradation, or the emergence of multiple cracks. Incorporating these additional damage scenarios would strengthen the overall robustness of the monitoring system. The updated finite element model could be used in time-based analyses to obtain acceleration signals, allowing for the testing of simplified damage detection algorithms. Finally, exploring transfer learning for application to similar structures could accelerate the training of predictive models. Objective criteria, such as modal shape similarity, could be employed to evaluate structural comparability, thereby facilitating effective knowledge transfer while preserving key aspects of the methodology proposed in this work.

11.
References

1. Ho LV, Nguyen DH, Mousavi M, et al (2021) A hybrid computational intelligence approach for structural damage detection using marine predator algorithm and feedforward neural networks. Comput Struct 252:. https://doi.org/10.1016/j.compstruc.2021.106568
2. An Y, Chatzi E, Sim S, et al (2019) Recent progress and future trends on damage identification methods for bridge structures. Struct Control Health Monit 26:1–30. https://doi.org/10.1002/stc.2416
3. Entezami A, Sarmadi H, Behkamal B, Mariani S (2025) Early warning of structural damage via manifold learning-aided data clustering and non-parametric probabilistic anomaly detection. Mech Syst Signal Process 224:. https://doi.org/10.1016/j.ymssp.2024.111984
4. Carden EP, Fanning P (2004) Vibration Based Condition Monitoring: A Review. Struct Health Monit 3:355–377. https://doi.org/10.1177/1475921704047500
5. Tibaduiza Burgos DA, Gomez Vargas RC, Pedraza C, et al (2020) Damage Identification in Structural Health Monitoring: A Brief Review from its Implementation to the Use of Data-Driven Applications. Sensors 20:733. https://doi.org/10.3390/s20030733
6. Niyirora R, Ji W, Masengesho E, et al (2022) Intelligent damage diagnosis in bridges using vibration-based monitoring approaches and machine learning: A systematic review. Results in Engineering 16:100761. https://doi.org/10.1016/j.rineng.2022.100761
7. Davila Delgado JM, Butler LJ, Gibbons N, et al (2017) Management of structural monitoring data of bridges using BIM. Proceedings of the Institution of Civil Engineers - Bridge Engineering 170:204–218. https://doi.org/10.1680/jbren.16.00013
8. Oliveira JGP, de França Moura JM, dos S. Mota V, et al (2025) Dynamic testing and finite element model updating for a viaduct structural assessment. J Civ Struct Health Monit. https://doi.org/10.1007/s13349-025-00940-y
9. Rainieri C, Fabbrocino G (2014) Operational Modal Analysis of Civil Engineering Structures. Springer New York, New York, NY

10. Rodrigues, Jorge (2005) Identificação modal estocástica métodos de análise e aplicações em estruturas de engenharia civil. Thesis, Universidade do Porto
11. Sabamehr A, Lim C, Bagchi A (2018) System identification and model updating of highway bridges using ambient vibration tests. J Civ Struct Health Monit 8:755–771. https://doi.org/10.1007/s13349-018-0304-5
12. Masciotta MG, Ramos LF (2018) Dynamic identification of historic masonry structures. In: Long-term Performance and Durability of Masonry Structures: Degradation Mechanisms, Health Monitoring and Service Life Design. Elsevier, pp 241–264
13. Brincker R;, Ventura CE, Andersen P (2001) Damping Estimation by Frequency Domain Decomposition. In: IMAC 19: A Conference on Structural Dynamics. Kissimmee, pp 698–703
14. Brincker R;, Zhang L;, Andersen P (2000) Modal Identification from Ambient Responses using Frequency Domain Decomposition. In: International Modal Analysis Conference (IMAC). San Antonio, pp 625–630
15. Bendat JS, Piersol AG (2010) Random Data, Fourth Edition. Wiley, Hoboken
16. Brincker R (2014) Some Elements of Operational Modal Analysis. Shock and Vibration 2014:1–11. https://doi.org/10.1155/2014/325839
17. Magalhães F, Cunha A, Caetano E (2012) Vibration based structural health monitoring of an arch bridge: From automated OMA to damage detection. Mech Syst Signal Process 28:212–228. https://doi.org/10.1016/j.ymssp.2011.06.011
18. Magalhães F, Cunha Á (2011) Explaining operational modal analysis with data from an arch bridge. Mech Syst Signal Process 25:1431–1450. https://doi.org/10.1016/j.ymssp.2010.08.001
19. Reynders E, Maes K, Lombaert G, De Roeck G (2016) Uncertainty quantification in operational modal analysis with stochastic subspace identification: Validation and applications. Mech Syst Signal Process 66–67:13–30. https://doi.org/10.1016/j.ymssp.2015.04.018
20. Chauhan S (2016) Subspace Algorithms in Modal Parameter Estimation for Operational Modal Analysis: Perspectives and Practices. In: Rotating Machinery, Hybrid Test Methods, Vibro-Acoustics & Laser Vibrometry. pp 295–301
21. Qin S, Kang J, Wang Q (2016) Operational Modal Analysis Based on Subspace Algorithm with an Improved Stabilization Diagram Method. Shock and Vibration 2016:1–10. https://doi.org/10.1155/2016/7598965

22. Peeters B, De Roeck G (2001) One-year monitoring of the Z24-Bridge: environmental effects versus damage events. Earthq Eng Struct Dyn 30:149–171. https://doi.org/10.1002/1096-9845(200102)30:2<149::AID-EQE1>3.0.CO;2-Z
23. Peeters B (2000) System Identification and Damage Detection in Civil Engineering
24. Simoen E, De Roeck G, Lombaert G (2015) Dealing with uncertainty in model updating for damage assessment: A review. Mech Syst Signal Process 56–57:123–149. https://doi.org/10.1016/j.ymssp.2014.11.001
25. Svendsen BT, Øiseth O, Frøseth GT, Rønnquist A (2023) A hybrid structural health monitoring approach for damage detection in steel bridges under simulated environmental conditions using numerical and experimental data. Struct Health Monit 22:540–561. https://doi.org/10.1177/14759217221098998
26. Pandey AK, Biswas M, Samman MM (1991) Damage detection from changes in curvature mode shapes. J Sound Vib 145:321–332. https://doi.org/10.1016/0022-460X(91)90595-B
27. Nick H, Aziminejad A, Hamid Hosseini M, Laknejadi K (2021) Damage identification in steel girder bridges using modal strain energy-based damage index method and artificial neural network. Eng Fail Anal 119:. https://doi.org/10.1016/j.engfailanal.2020.105010
28. Abdel Wahab MM, De Roeck G (1999) Damage detection in bridges using modal curvatures: application to a real damage scenario. J Sound Vib 226:217–235. https://doi.org/10.1006/jsvi.1999.2295
29. Dilena M, Limongelli MP, Morassi A (2015) Damage localization in bridges via the FRF interpolation method. Mech Syst Signal Process 52–53:162–180. https://doi.org/10.1016/j.ymssp.2014.08.014
30. Erduran E, Ulla FK, Næss L (2021) A framework for long-term vibration-based monitoring of bridges. Sensors 21:. https://doi.org/10.3390/s21144739
31. Sánchez-Aparicio LJ, Ramos LF, Sena-Cruz J, et al (2015) Experimental and numerical approaches for structural assessment in new footbridge designs (SFRSCC-GFPR hybrid structure). Compos Struct 134:95–105. https://doi.org/10.1016/j.compstruct.2015.07.041
32. Stubbs N, Kim J-T (1996) Damage localization in structures without baseline modal parameters. AIAA Journal 34:1644–1649. https://doi.org/10.2514/3.13284

33. Jayasundara N, Thambiratnam D, Chan T, Nguyen A (2019) Vibration-based dual-criteria approach for damage detection in arch bridges. Struct Health Monit 18:2004–2019. https://doi.org/10.1177/1475921718810011
34. Zalaghi S, Aziminejad A, Rahami H, et al (2024) Damage Identification in Steel Girders of Highway Bridges Utilizing Vibration Based Methods and Convolution Neural Network in the Presence of Noise. J Nondestr Eval 43:. https://doi.org/10.1007/s10921-024-01057-w
35. Tan ZX, Thambiratnam DP, Chan THT, et al (2020) Damage detection in steel-concrete composite bridge using vibration characteristics and artificial neural network. Structure and Infrastructure Engineering 16:1247–1261. https://doi.org/10.1080/15732479.2019.1696378
36. Entezami A, Shariatmadar H (2014) Damage detection in structural systems by improved sensitivity of modal strain energy and Tikhonov regularization method. Int J Dyn Control 2:509–520. https://doi.org/10.1007/s40435-014-0071-z
37. Dong J, Wang Q, Guan Z (2013) Structural behaviour of RC beams with external flexural and flexural–shear strengthening by FRP sheets. Compos B Eng 44:604–612. https://doi.org/10.1016/j.compositesb.2012.02.018
38. Wickramasinghe WR, Thambiratnam DP, Chan THT, Nguyen T (2016) Vibration characteristics and damage detection in a suspension bridge. J Sound Vib 375:254–274. https://doi.org/10.1016/j.jsv.2016.04.025
39. Dawari VB, Vesmawala GR (2013) Modal Curvature and Modal Flexibility Methods for Honeycomb Damage Identification in Reinforced Concrete Beams. Procedia Eng 51:119–124. https://doi.org/10.1016/j.proeng.2013.01.018
40. Ndambi J-M, Vantomme J, Harri K (2002) Damage assessment in reinforced concrete beams using eigenfrequencies and mode shape derivatives. Eng Struct 24:501–515. https://doi.org/10.1016/S0141-0296(01)00117-1
41. Rosales MB, Filipich CP, Buezas FS (2009) Crack detection in beam-like structures. Eng Struct 31:2257–2264. https://doi.org/10.1016/j.engstruct.2009.04.007
42. dos Santos Mota V, Lima Corrêa de Albuquerque N, Marques Gaspar CR, Dominguez Sotelino E (2023) Modal Identification of Damage in the Dowling Hall Pedestrian Footbridge. In: XLIV Ibero-Latin American Congress on Computational Methods in Engineering. ABMEC, Porto

43. Altunisik AC, Bayraktar A (2017) Manual model updating of highway bridges under operational condition. Smart Struct Syst 19:39–46. https://doi.org/10.12989/sss.2017.19.1.039
44. De Angelis A, Pecce MR (2023) Model assessment of a bridge by load and dynamic tests. Eng Struct 275:. https://doi.org/10.1016/j.engstruct.2022.115282
45. Talebi A, Potenza F, Gattulli V (2023) Interoperability between BIM and FEM for vibration-based model updating of a pedestrian bridge. Structures 53:1092–1107. https://doi.org/10.1016/j.istruc.2023.04.115
46. Brownjohn JMW, Xia P-Q, Hao H, Xia Y (2001) Civil structure condition assessment by FE model updating: Finite Elements in Analysis and Design 37:761–775. https://doi.org/10.1016/S0168-874X(00)00071-8
47. Garcia-Palencia AJ, Santini-Bell E, Sipple JD, Sanayei M (2015) Structural model updating of an in-service bridge using dynamic data. Struct Control Health Monit 22:1265–1281. https://doi.org/10.1002/stc.1742
48. Malveiro J, Ribeiro D, Sousa C, Calçada R (2018) Model updating of a dynamic model of a composite steel-concrete railway viaduct based on experimental tests. Eng Struct 164:40–52. https://doi.org/10.1016/j.engstruct.2018.02.057
49. Ren WX, Chen HB (2010) Finite element model updating in structural dynamics by using the response surface method. Eng Struct 32:2455–2465. https://doi.org/10.1016/j.engstruct.2010.04.019
50. Svendsen BT, Petersen ØW, Frøseth GT, Rønnquist A (2022) Improved finite element model updating of a full-scale steel bridge using sensitivity analysis. Structure and Infrastructure Engineering 19:315–331. https://doi.org/10.1080/15732479.2021.1944227
51. Liu M, Sun Q, Yu H, et al (2021) Static and dynamic test analysis of a 12-years old 14 000-ton cable-stayed bridge used swivel construction technology. Archives of Civil Engineering 67:369–381. https://doi.org/10.24425/ace.2021.138505
52. Schlune H, Plos M, Gylltoft K (2009) Improved bridge evaluation through finite element model updating using static and dynamic measurements. Eng Struct 31:1477–1485. https://doi.org/10.1016/j.engstruct.2009.02.011
53. Allemang RJ (2002) The Modal Assurance Criterion – Twenty Years of Use and Abuse. In: 20th International Modal Analysis Conference. pp 14–21

54. Watson RT, Webster J (2020) Analysing the past to prepare for the future: Writing a literature review a roadmap for release 2.0. J Decis Syst 29:129–147. https://doi.org/10.1080/12460125.2020.1798591
55. Pati D, Lorusso LN (2018) How to Write a Systematic Review of the Literature. HERD: Health Environments Research & Design Journal 11:15–30. https://doi.org/10.1177/1937586717747384
56. McGuire B, Atadero R, Clevenger C, Ozbek M (2016) Bridge Information Modeling for Inspection and Evaluation. Journal of Bridge Engineering 21:. https://doi.org/10.1061/(asce)be.1943-5592.0000850
57. McKenna T, Minehane M, O'Keeffe B, et al (2017) Bridge information modelling (BrIM) for a listed viaduct. Proceedings of the Institution of Civil Engineers: Bridge Engineering 170:192–203. https://doi.org/10.1680/jbren.16.00007
58. Sacks R, Kedar A, Borrmann A, et al (2018) SeeBridge as next generation bridge inspection: Overview, Information Delivery Manual and Model View Definition. Autom Constr 90:134–145. https://doi.org/10.1016/j.autcon.2018.02.033
59. Wan C, Zhou Z, Li S, et al (2019) Development of a bridge management system based on the building information modeling technology. Sustainability (Switzerland) 11:. https://doi.org/10.3390/su11174583
60. Boddupalli C, Sadhu A, Rezazadeh Azar E, Pattyson S (2019) Improved visualization of infrastructure monitoring data using building information modeling. Structure and Infrastructure Engineering 15:1247–1263. https://doi.org/10.1080/15732479.2019.1602150
61. Singh P, Sadhu A (2020) System Identification-Enhanced Visualization Tool for Infrastructure Monitoring and Maintenance. Front Built Environ 6:. https://doi.org/10.3389/fbuil.2020.00076
62. Kwon TH, Park SH, Park SI, Lee SH (2021) Building information modeling-based bridge health monitoring for anomaly detection under complex loading conditions using artificial neural networks. J Civ Struct Health Monit 11:1301–1319. https://doi.org/10.1007/s13349-021-00508-6
63. Kaewunruen S, Sresakoolchai J, Ma W, Phil-Ebosie O (2021) Digital twin aided vulnerability assessment and risk-based maintenance planning of bridge infrastructures exposed to extreme conditions. Sustainability (Switzerland) 13:1–19. https://doi.org/10.3390/su13042051

64. Hamdan AH, Taraben J, Helmrich M, et al (2021) A semantic modeling approach for the automated detection and interpretation of structural damage. Autom Constr 128:. https://doi.org/10.1016/j.autcon.2021.103739
65. Yamane T, Chun P, Honda R (2024) Detecting and localising damage based on image recognition and structure from motion, and reflecting it in a 3D bridge model. Structure and Infrastructure Engineering 20:594–606. https://doi.org/10.1080/15732479.2022.2131845
66. Li X, Xiao Y, Guo H, Zhang J (2022) A BIM Based Approach for Structural Health Monitoring of Bridges. KSCE Journal of Civil Engineering 26:155–165. https://doi.org/10.1007/s12205-021-2040-3
67. Truong M-P, Dang N-L, Cao V-T, Ngo T-C (2023) Building information modeling integrated with damage detection algorithm for structural health monitoring of bridge. IOP Conf Ser Mater Sci Eng 1289:012039. https://doi.org/10.1088/1757-899x/1289/1/012039
68. Petti L, Lupo C, De Gaetano CM (2023) A Methodological Framework for Bridge Surveillance. Applied Sciences (Switzerland) 13:. https://doi.org/10.3390/app13084975
69. Mohammadi M, Rashidi M, Yu Y, Samali B (2023) Integration of TLS-derived Bridge Information Modeling (BrIM) with a Decision Support System (DSS) for digital twinning and asset management of bridge infrastructures. Comput Ind 147:. https://doi.org/10.1016/j.compind.2023.103881
70. Mohamed AG, Khaled A, Abotaleb IS (2023) A Bridge Information Modeling (BrIM) Framework for Inspection and Maintenance Intervention in Reinforced Concrete Bridges. Buildings 13:2798. https://doi.org/10.3390/buildings13112798
71. Fawad M, Salamak M, Poprawa G, et al (2023) Automation of structural health monitoring (SHM) system of a bridge using BIMification approach and BIM-based finite element model development. Sci Rep 13:13215. https://doi.org/10.1038/s41598-023-40355-7
72. Gragnaniello C, Mariniello G, Pastore T, Asprone D (2024) BIM-based design and setup of structural health monitoring systems. Autom Constr 158:105245. https://doi.org/10.1016/j.autcon.2023.105245
73. Hagedorn P, Liu L, König M, et al (2023) BIM-Enabled Infrastructure Asset Management Using Information Containers and Semantic Web. Journal of Computing in Civil Engineering 37:. https://doi.org/10.1061/(asce)cp.1943-5487.0001051

74. Aziz Z, Riaz Z, Arslan M (2017) Leveraging BIM and Big Data to deliver well maintained highways. Facilities 35:818–832. https://doi.org/10.1108/F-02-2016-0021
75. Alsharif MA, Thermou G, Ninic J, Tizani W (2025) Data integration framework for multi-level information modelling and numerical analysis of deteriorated RC bridges. Advances in Engineering Software 202:. https://doi.org/10.1016/j.advengsoft.2024.103860
76. Lu R, Brilakis I (2019) Digital twinning of existing reinforced concrete bridges from labelled point clusters. Autom Constr 105:102837. https://doi.org/10.1016/j.autcon.2019.102837
77. Kritzinger W, Karner M, Traar G, et al (2018) Digital Twin in manufacturing: A categorical literature review and classification. In: IFAC-PapersOnLine. Elsevier B.V., pp 1016–1022
78. Honghong S, Gang Y, Haijiang L, et al (2023) Digital twin enhanced BIM to shape full life cycle digital transformation for bridge engineering. Autom Constr 147:104736. https://doi.org/10.1016/j.autcon.2022.104736
79. van Eldik MA, Vahdatikhaki F, dos Santos JMO, et al (2020) BIM-based environmental impact assessment for infrastructure design projects. Autom Constr 120:. https://doi.org/10.1016/j.autcon.2020.103379
80. Deng L, Lai S, Ma J, et al (2022) Visualization and monitoring information management of bridge structure health and safety early warning based on BIM. Journal of Asian Architecture and Building Engineering 21:427–438. https://doi.org/10.1080/13467581.2020.1869013
81. Yi L, Deng X, Yang LT, et al (2021) Reinforcement-Learning-Enabled Partial Confident Information Coverage for IoT-Based Bridge Structural Health Monitoring. IEEE Internet Things J 8:3108–3119. https://doi.org/10.1109/JIOT.2020.3028325
82. Heykoop I, Hoult N, Woods JE, Fernando H (2024) Development and field evaluation of a low-cost bridge bearing movement monitoring system. J Civ Struct Health Monit 14:931–946. https://doi.org/10.1007/s13349-024-00771-3
83. Scianna A, Gaglio GF, La Guardia M (2022) Structure Monitoring with BIM and IoT: The Case Study of a Bridge Beam Model. ISPRS Int J Geoinf 11:. https://doi.org/10.3390/ijgi11030173
84. Huang D, Lu Y, Hua L, et al (2024) Building information modeling supported bridge structural health diagnosis and prognosis. Struct Health Monit. https://doi.org/10.1177/14759217241293460

85. Girardet A, Boton C (2021) A parametric BIM approach to foster bridge project design and analysis. Autom Constr 126:. https://doi.org/10.1016/j.autcon.2021.103679
86. Zhang XY, Qu QL, Liang D, Liu TC (2022) Endowing BIM Model with Mechanical Properties-Finite Element Simulation Analysis of Long-Span Corrugated Steel Web Continuous Beam Bridge. In: Journal of Physics: Conference Series. IOP Publishing Ltd
87. Chung W, Sotelino ED (2006) Three-dimensional finite element modeling of composite girder bridges. Eng Struct 28:63–71. https://doi.org/10.1016/j.engstruct.2005.05.019
88. Gordan M, Razak HA, Ismail Z, et al (2020) A hybrid ANN-based imperial competitive algorithm methodology for structural damage identification of slab-on-girder bridge using data mining. Applied Soft Computing Journal 88:106013. https://doi.org/10.1016/j.asoc.2019.106013
89. Jayasundara N, Thambiratnam DP, Chan THT, Nguyen A (2020) Damage detection and quantification in deck type arch bridges using vibration based methods and artificial neural networks. Eng Fail Anal 109:104265. https://doi.org/10.1016/j.engfailanal.2019.104265
90. Fan W, Chen Y, Li J, et al (2021) Machine learning applied to the design and inspection of reinforced concrete bridges: Resilient methods and emerging applications. Structures 33:3954–3963. https://doi.org/10.1016/j.istruc.2021.06.110
91. Wei Fan, Pizhong Qiao (2011) Vibration-based Damage Identification Methods: A Review and Comparative Study. Struct Health Monit 10:83–111. https://doi.org/10.1177/1475921710365419
92. Farrar CR, James III GH (1997) SYSTEM IDENTIFICATION FROM AMBIENT VIBRATION MEASUREMENTS ON A BRIDGE. J Sound Vib 205:1–18. https://doi.org/10.1006/jsvi.1997.0977
93. Peeters B, Roeck G De (2001) Stochastic system identification for operational modal analysis: A Review. Journal of Dynamic Systems, Measurement and Control, Transactions of the ASME 123:659–667. https://doi.org/10.1115/1.1410370
94. Dassault Systèmes (2018) Abaqus 2019 Documentation
95. Xu H, Humar J (2006) Damage Detection in a Girder Bridge by Artificial Neural Network Technique
96. Gómez Araújo I, Laier JE, Carrazedo R (2019) Enhanced Power Spectral Density Transmissibility Matrix for Operational Modal Analysis of Structures.

Journal of Structural Engineering 145:. https://doi.org/10.1061/(asce)st.1943-541x.0002322

97. National Instruments (2015) SignalExpress
98. Structural Vibration Solutions A. (2018) ARTeMIS Modal
99. Sepe V, Diaferio M, Caraccio R (2024) Safety Evaluation of Existing R.C. Buildings: Uncertainties Due to the Location of In Situ Tests. Applied Sciences (Switzerland) 14:. https://doi.org/10.3390/app14072749
100. Maracchini G, Clementi F, Quagliarini E, et al (2017) Preliminary study of the influence of different modelling choices and materials properties uncertainties on the seismic assessment of an existing RC school building. In: AIP Conference Proceedings. American Institute of Physics Inc.
101. National Department of Transportation Infrastructure of Brazil (2021) Quadro de Fabricantes de Veículos. DNIT, Brasilia
102. Gentile C, Gallino N (2008) Ambient vibration testing and structural evaluation of an historic suspension footbridge. Advances in Engineering Software 39:356–366. https://doi.org/10.1016/j.advengsoft.2007.01.001
103. Lee S, Feng MQ, Kwon S-J, Hong S-H (2011) Equivalent Modal Damping of Short-Span Bridges Subjected to Strong Motion. Journal of Bridge Engineering 16:316–323. https://doi.org/10.1061/(ASCE)BE.1943-5592.0000149
104. Doebling SW, Farrar CR, Prime MB, Shevitz DW (1996) Damage identification and health monitoring of structural and mechanical systems from changes in their vibration characteristics: A literature review. Los Alamos, NM
105. Cremona C (2004) Dynamic monitoring applied to the detection of structural modifications: a high-speed railway bridge study. Progress in Structural Engineering and Materials 6:147–161. https://doi.org/10.1002/pse.177
106. Zini G, Giachetti A, Betti M, Bartoli G (2024) Vibration signature effects on damping identification of a RC bridge under ambient vibrations. Eng Struct 298:. https://doi.org/10.1016/j.engstruct.2023.116934
107. Teughels A, De Roeck G (2004) Structural damage identification of the highway bridge Z24 by FE model updating. J Sound Vib 278:589–610. https://doi.org/10.1016/j.jsv.2003.10.041